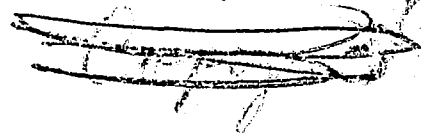TECHNICAL MEMORANDUMS

NATIONAL ADVISORY COMMITTEE FOR AERONAUTICS

No. 874

EFFECT OF PROPELLER SLIPSTREAM ON WING AND TAIL

By J. Stüper

Washington
August 1938

NATIONAL ADVISORY COMMITTEE FOR AERONAUTICS

TECHNICAL MEMORANDUM NO. 874

EFFECT OF PROPELLER SLIPSTREAM ON WING AND TAIL*

By J. Stüper

The results of wind-tunnel tests for the determina-
tion of the effect of a jet on the lift and downwash of a
wing are presented in this report. In the first part, a
jet without rotation and with constant velocity distribu-
tion is considered - the jet being produced by a specially
designed fan. Three-component, pressure distribution, and
downwash measurements were made and the results compared
with existing theory. The effect of a propeller slipstream
was investigated in the second part. In the two cases the
jet axis coincided with the undisturbed wind direction. In
the third part the effect of the inclination of the propel-
ler axis to the wing chord was considered, the results be-
ing obtained for a model wing with running propeller.

I. INTRODUCTION

    Attempts that have hitherto been made at constructing
a useful theory of the longitudinal stability of an air-
plane in powered flight, have all come up against the dif-
ficulty involved in the fact that the effect of the pro-
peller slipstream on wing and tail has not yet been suffi-
ciently investigated. In the present paper a study is made
of the mutual interaction of propeller, wing, and tail -
the fuselage effect for the present not being investigated.
The order of the three elements considered, namely, pro-
peller, wing, and tail thus corresponds to the arrangement
of multi-engine airplanes with side engines. The problems
to be solved are the two following:

    a) The effect of the propeller slipstream on the wing
         lift distribution;

    b) The effect of the propeller slipstream on the veloc-
         ity and direction of the flow at the tail loca-
         tion.

_____

The variable parameters of chief importance are: the angle of attack, the setting of the propeller axis to the zero-lift direction of the wing, the angle between the propeller axis and the relative wind direction, and the propeller V/nD and thrust coefficient. The vertical position of the wing in the jet was not varied in our tests, the propeller axis always being on a level with the wing. The side engines in present-day airplanes are mounted exclusively in this manner, and in individual types the differences in the vertical locations of the engines amount at most to a value of the order of the wing-section thickness. As has been shown by both theory and experiment (reference 24), a slight displacement of this kind produces no effect on the lift relations.

TABLE I

Airplane		$\dfrac{2R}{t}$	$\dfrac{E}{t}$	$\dfrac{2A}{b}$
Do 17		0.92	0.52	0.28
He 111		.68	.34	.23
Ju 86		.74	.27	.25
Lockheed 12		1.02	.46	.27
Lockheed 14		.84	.45	.28
Boeing 247-D		.68	.43	.21
Burnelli UB-14		.66	.41	.15
Douglas DC 3		.82	.43	.19
Douglas DC 4	inside	.60	.33	.19
	outside	.72	.40	.41
Ha 139	inside	.76	.21	.23
	outside	.76	.21	.49
Martin 130	inside	.30	.26	.13
	outside	.28	.25	.32
Martin 156	inside	.32	.31	.11
	outside	.34	.32	.29
Sikorsky S-42	inside	.42	.24	.12
	outside	.42	.24	.33

Table I gives dimension ratios of the most important representatives of modern multi-engine airplanes, the notation being indicated on figure 1. It is evident, from an inspection of the table, that in spite of the variety of the types of airplanes, the numerical values indicated vary only within narrow limits. The effect of a jet on a wing for the case where the outside air velocity is zero - that is, the problem of a wing spanning a free jet - has been extensively investigated both theoretically and experimen-

tally (references 3, 10, 18, 19, 21, 23, and 24). The case where the external air is in motion was treated theoretically by C. Ferrari (reference 7) and C. Koning (reference 14). Ferrari neglected to take into account the boundary condition that must be satisfied at the jet-boundary surface. He found that the circulation of the wing was not changed by the propeller slipstream, so that the increase in lift in the jet was proportional to the increase in the velocity in the jet. Koning determined the jet effect for the case where the jet-boundary condition was satisfied. On account of the great mathematical difficulties involved, however, he was forced to make the following simplifying assumptions. The angle between the relative wind direction and the jet axis was equal to zero; the jet was free from rotational components and had constant velocity distribution over the cross section and along the jet axis. Furthermore, it was necessary to assume that the additional velocity in the jet was small compared with the main tunnel velocity in order that the problem might be "linearized." A comparison of the investigations of Ferrari and Koning gives the remarkable result, namely, that the relatively rough computation of Ferrari leads to the correct value for the _total_ increase in lift produced by the propeller slipstream, but that the added _lift distribution_ over the span deviates strongly from the actual distribution. Thus is explained the good agreement of Ferrari's computations with the results of measurements where the distribution of the lift is not taken into account. Neither theory is capable of giving any clear predictions as to the actual downwash relations.

The simplified assumptions of the theory of Koning limit its usefulness for practical application. On the other hand, since the great multiplicity of factors involved — nonuniformity of velocity distribution and rotation in the jet, mixing region at the jet boundary, inclination of propeller and jet to the relative wind, effect of the friction layer, etc. — make exhaustive theoretical treatment very difficult, if not impossible, the solution of the problem must first be sought along experimental lines. For the purpose of learning the effect of the individual parameters and their mutual interaction, the following investigation program was formulated:

1. Effect on a wing of a jet without rotation with constant velocity distribution, the relative wind direction and the jet axis coinciding (the case treated by Koning); three component measurements, determination of

the lift distribution by pressure-distribution measurements, determination of the downwash at the tail location.

2. Effect on a wing of propeller slipstream with rotation, the propeller axis and the relative wind direction coinciding; three-component and pressure-distribution measurements, determination of the downwash in magnitude and direction.

3. Interaction of wing and propeller. The angle between the propeller axis and the zero lift direction of the wing to be varied between $0°$ and $15°$. Three-component measurements and pressure-distribution measurements, determination of the downwash relations, effect of the propeller V/nD.

4. Investigations on a twin-engine airplane in flight; pressure-distribution measurements in propeller slipstream, downwash and longitudinal-stability measurements, with particular account taken of jet effect.

5. Six-component and pressure-distribution measurements on a model of a twin-engine airplane with propeller running; comparison with flight-test measurements, determination of effect of direction of propeller rotation on the downwash and stability relations; effect of angle between propeller axis and plane of symmetry of airplane.

6. Determination of the shielding effect of an airplane propeller operating with negative thrust.

The first three points of the above program are treated in the present report.

II. WIND-TUNNEL CORRECTION

The data presented in this report are the uncorrected wind-tunnel measurements, since for the purposes of this work the application of such correction was not considered necessary. For the sake of completeness, the values of the wind-tunnel corrections are given here. The correction $\Delta\alpha$, which must be applied to the angle of attack in order that the lift in the bounded tunnel flow equal that of the infinitely extended flow, may be expressed as follows:

$$\Delta\alpha = \frac{c_a}{8}\frac{F}{F_0}\delta*$$

where   F   is the wing area

     F_0,   tunnel cross-sectional area

     $\delta*$,   correction factor

For the case of the two model wings here considered:

$$F = 0.16 \text{ m}^2$$

so that with $F_0 = 1.765 \text{ m}^2$

$$F/F_0 = 0.0906$$

In the computations made along the tunnel axis there is obtained for the value at the center of the wings, taking into account the end disk effect at the wing location:

     a) $\delta* = 1.000$

so that $\Delta\alpha = 0.0113\ c_a$

     b)   For the mean value over the wing:

     $\delta* = 1.018$

and $\Delta\alpha = 0.0115\ c_a$

At the distance of 2.5 t behind the leading edge of the wing, there is obtained:

     $\delta* = 1.720$

and $\Delta\alpha = 0.0194\ c_a$

A further computation showed that the latter value did not change appreciably within the limits of variation of the vertical location of the measuring instruments for the determination of the downwash relations (vane, sphere, two-prong apparatus). It may be noted in this connection that in determining the drag, correction was always made for the drag of the end disks and fairings in addition to that of the suspension members.

III. EFFECT ON A WING OF A JET WITHOUT ROTATION WITH

CONSTANT VELOCITY DISTRIBUTION

Test Set-Up and Procedure

The measurements were made on a wing of symmetrical section (Göttingen 409) having a span b = 80 cm, chord t = 20 cm between two circular end disks of diameter h = 32 cm. Figure 2 shows the test set-up for obtaining the polar curves. The wing is suspended on a three-component balance in the wind tunnel of the propeller-research laboratory. In front of the wing is the fan for producing the rotation-free jet. Figure 3 shows a cross section of the blower. The main rotational components of the jet produced by propeller a are removed by the vanes b. The honeycomb d further straightens the jet while the constancy of the velocity distribution is obtained by suitable choice of the mesh e. The throat f with the exit diameter 2R = 12 cm has a slight flare at the end in order to oppose the jet contraction. Figures 4 and 5 show the dynamic pressure distribution for the two operating conditions under which the tests were conducted (q = dynamic pressure of undisturbed flow, $q_\oslash$ = dynamic pressure in jet). The measurements were made in the plane bisected by the jet at various distances x from the plane of the throat outlet. Particularly to be noted is the only very slight increase in the extent of the mixing zone with increasing distance from the throat. The velocity of the undisturbed flow V_∞ for all the measurements amounted to 30 m/s (67 m.p.h.). The relative increase s in the velocity in the equation:

$$V = (1 + s) \, V_\infty$$

(V is the velocity in the jet) has the values, respectively, 0.18 and 0.36. The friction boundary layer of the fan enclosure produces a dynamic pressure drop in the transition region between jet and undisturbed flow. It is to be assumed that this cylinder of slowed-down velocity acts as a certain shield against the interference of the flow processes within and outside the jet. The jet was found to be free from rotation.

In all the measurements the wing was located at the center of the jet; the changes in the angle of attack were effected by rotating the wing about the leading edge. Two

series of measurements were made at distances of 0.25 chord and 0.5 chord between the exit plane of the throat and the wing leading edge. The results obtained were identical within the limits of accuracy. The other measurements were then continued at a distance of 0.25 chord.

Test Results

Figure 6 shows the lift as a function of the angle of attack. The jet gives rise to an increase in the lift slope $\frac{dc_a}{d\alpha}$, which increase, however, is not proportional to the increase in the velocity. The maximum lift increases and flow separation is delayed to higher angles of attack. This phenomenon is to be explained by the effect on the jet of the boundary friction layer of the wing, the jet acting to delay separation. Whereas in the case of the wing without the jet the flow separation starts at the wing center, it is found that with the jet acting on the wing, separation starts outside of the jet region. This fact is of importance. In the design of an airplane the plan form and twisting of the wing are so determined that in flight at high angles of attack separation starts at the wing center in order to prevent dangerous banking of the wing. This computation is generally conducted without taking into account the propeller slipstream. Now the effect of the slipstream is to support the flow at the center and the wing is again exposed to the danger of wingtip stalling. The condition corresponding to power-on flight at large angles of attack is met with not only in take-off and climb but also in blind flying and in landing of seaplanes at full power on smooth water.

Figure 7 shows the polar and moment curves. The jet has no effect on the moment curve and the polar shows a constant increment of the drag as a result of the jet.

In order to be able to determine the effect of the jet on the lift distribution, 17 orifices were bored in each of 17 measuring stations along the span. Figure 8 shows the test set-up for the pressure-distribution measurements. The pressures at each of the measuring stations were photographically recorded with the aid of the multiple manometer seen in the foreground of the figure. The pressure distributions for the different angles of attack are given on figures 9, 10, 11, and 12, the pressures p/q_0 (where p is the static pressure at the station)

being plotted against the projections of the orifices on
the undisturbed wind direction as abscissas. The area in-
cluded by the pressure-distribution curves (obtained by
planimeter) is thus the lift contributed at each section.
The figures above the curves are the values of y/R (where
y is the spanwise coordinate) and hence indicate the posi-
tion of each section from the jet center. The lift dis-
tributions for the different angles of attack are shown
on figure 13. It may be seen that there is an increase in
the lift in the region of the jet but that in addition,
there is a large effect also on the portions of the wing
lying outside the jet. The strong decrease in the lift
is due to the friction boundary layer, already referred to,
of the fan enclosed.

          Comparison between Theory and Experiment

     The first attempt to determine mathematically the ef-
fect of the propeller slipstream on the lift distribution
of a wing was made by C. Koning (reference 14).

     It is convenient here to give a short account of the
theory. To determine the lift distribution of a wing in
parallel flow with propeller slipstream, the flow is di-
vided into the following different parts:

     1.   "Undisturbed flow," with the velocity V_∞.

     2.   "Propeller flow," the difference between flow 1
          and the flow which would exist if the propel-
          ler were acting in the absence of the wing.

     3.   "Wing flow," the change in flow caused by the
          wing in the parallel flow in the absence of
          the propeller.

     4.   "Additional airfoil flow," the flow produced by
          the change in circulation of the disturbance
          flow, related directly to the change in cir-
          culation around the wing, caused by the action
          of the propeller.

     5.   "Additional flow," the flow which is still to be
          added to flows 1, 2, 3, 4, in order that the
          boundary conditions may be satisfied.

     The conditions which must be satisfied at the bound-
ary are:

a)   The pressure must have the same value on each
     side of the boundary, since there are no exter-
     nal forces acting on the jet boundary.

b)   The component of the velocity normal to the bound-
     ary is equal to zero since the flow is free from
     sources and is steady.

Both conditions are satisfied by the flow components
1 and 2, but in general, not by the components 3 and 4.
In order that these conditions may be satisfied, it is nec-
essary to add the additional flow component 5, and the
difficulty of the problem is just in determining this com-
ponent. For the case here considered of a wing of finite
span lying aft of the propeller and intersecting the jet,
an exact solution cannot be given and it is necessary to
be satisfied with an approximation.

In order to be able to carry out the computation at
all, it was necessary for Koning to make a number of as-
sumptions which referred essentially to flow component 2.
Figure 14 shows the position of the wing relative to the
propeller (jet) and to the undisturbed wind direction
for the general case. In the table below the simplifica-
tions assumed in the theory are compared with the actual
conditions.

Parameter	Actual condition	Simplification by Koning's theory
Angle between propeller axis and wind direction	changes with angle of attack = $\alpha - \kappa$	zero
Form of jet	determined by jet contraction	cylindrical
Velocity distribution V_x: a) over the cross section	variable, falling off at the edge and center	constant; $V = (1+s) V_\infty$
b) along the jet axis	variable, in the plane of the propeller disk $V_{xo} = \frac{1}{2} V_{x\infty}$	constant
Velocity increase in the jet	up to $s \approx 0.8$	$s \ll 1$, so that terms in s^2 may be neglected
Jet structure	with rotation	without rotation

The theory also takes no account of the effect of the
jet on the processes in the frictional boundary layer of
the wing. It is evident that these restricting assump-
tions strongly limit the possibilities of practical appli-
cation of the theory.

The case considered by Koning cannot be exactly repro-
duced in any experiment. A strict proof of the theory
with the aid of the measurements conducted is therefore
not to be expected. The results nevertheless yield some
interesting data.

The continuous lines in figures 15 and 16 show the
lift distribution as computed by Koning's theory for the
wing and jet used in the test. For the wing without jet
(dotted curve) the lift distribution was computed by the
method of I. Lotz. In the region of the jet the measured
lift coefficients are smaller than is required by the theo-
ry. To a large extent this deviation is due to the loss
in dynamic pressure due to the friction layer of the blower
body as is also shown by the sharp drop in lift at the jet
boundary. Outside of the jet the test results as well as
the theory show the surprisingly large effect of the jet.
According to the theory, the relative increase in lift due
to the jet $\dfrac{\Delta c_a(y)}{c_{a_0}(y)}$ is independent of the angle of attack,
the variation of this value along the span for our case be-
ing shown in figure 17. If these values are compared with
the values of $\dfrac{\Delta c_a(y)}{c_{a_0}(y)}$ obtained from the measurements (fig.
18), the latter show considerable dependence on the angle
of attack. For this dependence on the angle of attack, two
reasons may be given. First, the effect of the loss in
dynamic pressure at the jet boundary depends very strongly
on the angle of attack as may be seen from figures 15 and
16. Secondly, the jet — whose diameter is smaller than
the wing chord ($2R/t = 0.6$) — is deformed with increasing
angle of attack, the jet expanding on the pressure side
and contracting on the suction side. The local lift in-
crease by the jet thus becomes smaller. It was possible
to verify the correctness of this supposition by tests
with a jet of water. By means of air bubbles the jet was
rendered visible, and thus the jet deformation caused by
a wing of varying chord could be observed. The better
agreement between theory and experiment at the larger an-
gles of attack is also apparent. The flow about the wing
without jet begins to break away, whereas in the presence

of the jet, separation occurs later, and this condition
gives rise to greater values of $\dfrac{\Delta c_a(y)}{c_{a_0}(y)}$.

To the simplifying assumptions of Koning, there is
thus to be added a still further restriction, namely, that
the ratio of wing chord to jet radius must be small enough
to maintain constancy of the jet cross section.

Downwash Measurements

In order to obtain information on the flow relations
at the location of the tail downwash measurements were
made in a plane at a distance of 2.5 chords behind the
wing leading edge. Since the case of a jet without rota-
tional velocity components with constant velocity distribu-
tion is of less practical importance, we considered it
sufficient in this case to determine the downwash angle
with the aid of a "feeler vane" only. This vane consisted
of a metal plate 30 cm long by 10 cm deep, suspended on a
scale behind the wing. Figure 19 shows the arrangement
for the downwash measurements behind the wing without fan;
the vane can also be made out on figure 2. The measurements
were made at four different vertical positions behind the
wing. Figure 20 shows the arrangement and the definition
of the symbols. The setting of the vane was so adjusted
that its lift vanished. Figure 21 gives the results of
the measurements. The jet causes an increase in the down-
wash angle.

IV. EFFECT OF THE PROPELLER SLIPSTREAM ON THE WING

Test Set-Up, Procedure, and Results

In the following investigations the jet from the fan
is replaced by that from a propeller. The test set-up is
shown on figure 22. A small high-speed electric motor en-
closed in a wooden fairing, drives the propeller. The
latter has a diameter $2R = 15$ cm, and a pitch $H/D = 0.4$
(fig. 23). The measurements were conducted at a propeller
advance ratio $\lambda = 0.15$. Larger values of λ were not
used since the propeller would give no increase in veloci-
ty on account of the wake of the streamlined body which
it would first be necessary for the propeller to acceler-
ate. Before the start of the measurements proper, the

propeller slipstream was investigated in the absence of the
wing. Figure 24 shows the variation of the angle of rota-
tion, and figure 25 shows the dynamic pressure at various
distances from the plane of the propeller disk. The dy-
namic pressure was measured with a Prandtl-type tube, and
the angle of rotation with a two-pronged instrument. In
all of these flow-angle measurements, the angle given is
always the inclination of the flow to the horizontal. The
propeller axis was fixed in the direction of the tunnel
air velocity, and the angle between the zero-lift direc-
tion of the wing and the propeller axis was thus equal to
the angle of attack. The distance between the plane of
the propeller disk and the wing leading edge was 0.375
chord.

The results of the three-component measurements are
given in figures 26 and 27. In this case, too, there is
an increase in the lift slope $dc_a/d\alpha$ as a result of the
jet. The two lift lines intersect, however, at the value
of the coefficient $c_a = 0.2$ (fig. 26). At smaller an-
gles of attack therefore, the propeller slipstream leads
to a decrease in the lift. This phenomenon has also been
observed from the results of various flight and model tests
with power on (references 15, 17, 20). A closer examina-
tion of this effect will be made in connection with the
study of the lift distribution. (See below.) As in the
case of the jet free from rotational components, the moment
curves of the wing are unchanged, whereas the polar shows
a constant increase in the drag. Also in the presence of
the propeller slipstream, separation of the flow on at-
taining large angles of attack first occurred outside the
region of the jet.

The lift distribution was obtained by means of pres-
sure-distribution measurements. The distribution curves
are shown on figures 28, 29, 30, and 31; figure 32 shows
the lift coefficients obtained from these. In the pres-
ence of the propeller slipstream, two factors are effective
in changing the lift of the wing, namely, the increase in
the dynamic pressure in the jet and the change in the rel-
ative wind direction due to the rotation of the propeller
slipstream. The effect of the increase in the dynamic
pressure is proportional to the lift and, hence, approxi-
mately proportional to the angle of attack, while the ef-
fect of the rotation is, in general, independent of the
angle of attack as long as the linear portion of the lift
curve is being considered. As may be seen from figures
24 and 25, the dynamic pressure increase and the jet rota-

tion act in the same sense (tending to increase the lift) on the right side (positive values of y), while on the left side the rotation angle and the increase in the dynamic pressure oppose each other in their effect on the wing. Whether the one or the other effect prevails, depends on the angle of attack as may be seen from figure 32. For angles of attack up to about 8° the effect of the rotation angle is predominant - the propeller slipstream producing on the left portion a decrease in lift as compared with the wing in the absence of the propeller. This effect may therefore be strong enough so that for the smaller angles of attack the total change in lift may even become negative as a result of the propeller slipstream.

Downwash Measurements

With the arrangement indicated above for the feeler vane (figs. 22 and 33), the downwash was measured at the location of the tail. The results presented in figure 34 show an unexpected decrease in the downwash angle due to the propeller slipstream. This result which, on repeating the test, proved to be reproducible, stands in contradiction to practical experience and model tests (reference 5), which always give an increase in the downwash angle. The explanation is probably to be found in the fact that while the total lift at the vane vanishes, the lift may not vanish locally everywhere. The measuring vane is relatively large compared with the jet dimensions (vane span 30 cm, propeller diameter 15 cm), so that a considerable portion of the vane lies in the upwash near the jet. In the case of the model measurements referred to above, the tail was located entirely in the propeller slipstream.

In order to study with sufficient accuracy the effect of the propeller slipstream on the flow at the tail, and also to investigate the jet itself, a survey of the flow field in magnitude and direction was made in a plane normal to the wind direction at $2\frac{1}{2}$ chords behind the leading edge of the wing. Figure 35 shows the location of the measuring plane. As a control and for applying a correction, there was first measured the flow direction from the tunnel alone, the tunnel flow being found free from rotational components. There was then determined the downwash angle behind the wing in the absence of the propeller at the two positions $y/t = \pm 0.533$ (fig. 36). The "valleys" shown on the curves as shifting upward with increasing angle of attack are due to the downwash from the wing.

The downwash relations for the various angles of attack
are given in figures 37, 38, 39, 40, and 41. The cross-
hatched areas represent the change in the dynamic pres-
sure; they bring out the fact, particularly noteworthy,
that the propeller slipstream is cut by the wing into two
parts which do not again unite into a single jet. In ac-
cordance with the jet rotation, the upper portion is devi-
ated to the left and the lower portion to the right. Com-
parison with figures 24 and 36 shows that the wing removes
a considerable portion of the rotational motion in the
propeller slipstream and thus acts to some extent as a
flow straightener.

V. MUTUAL INTERACTION OF WING AND PROPELLER

Test Set-Up and Procedure

     In the following tests a study was made of the mutual
interaction of wing and propeller, the angle between the
zero-lift direction and the propeller axis being varied
between $0°$ and $15°$. For this purpose it was necessary to
make an arrangement whereby the propeller and wing could
interact without any outside disturbance. An undesirable
effect would have been obtained, for example, if the driv-
ing motor for the propeller were located in a nacelle at
the wing. The previously employed arrangement of enclos-
ing the motor in a fairing ahead of the wing would, in
the present case, have led to difficulties in mounting and
undesired effects on the flow since, with changes in angle
of attack of the wing, the propeller axis would correspond-
ingly have to be rotated along. The inclined flow on the
motor body would have given rise to considerable disturb-
ance.

     Figure 42 shows the model used in the test. The mo-
tor is attached outside of the flow to an end disk and
drives the propeller through a pair of bevel gears and a
shaft located in the wing. Figure 43 shows the wing with-
out, and figure 44 with, motor enclosed in the fairing.
The wing, of profile section Göttingen 398, has a span
$b = 80$ cm and a chord $t = 20$ cm, with end disk diameter
$h = 32$ cm. Figure 45 shows the lift curve of the wing
alone, and figure 46, the polar. The coefficients are
given in table II. To carry out the pressure-distribution
measurements, 20 measuring stations with 14 orifices each
were distributed over the span. The propeller shaft was

located in a bearing piece (fig. 42). By interchanging this bearing with others, it was possible to obtain different settings κ of the wing chord to the propeller axis. Four such pieces were used (fig. 47). On figure 48 are indicated the two extreme positions of the propeller axis and the definition of κ; the four values of κ used were 9°, 4°, -1°, and -6°.

The propeller used in these tests is shown on figure 49, and its thrust, torque, and efficiency curves are given on figure 50. With the arrangement employed, $H/D = 1.0$ and $2R/t = 1.034$. In the three-component measurements the values of λ used were 0.13, 0.16, 0.20, 0.35, and 0.55; while in the pressure-distribution and downwash measurements the value of 0.13 was omitted. The tunnel air velocity in all cases was 30 m/s.

Test Results

The numerical values of the three-component measurements are given in table III. Figures 51, 52, 53, and 54 show the variation of the lift with angle of attack. For the purpose of discussion of the results, it is to be noted that the total lift measured on the scale was made up of four component parts:

1. The lift from the wing itself, A_W

2. The lift at the wing due to the propeller slip-stream, A_{St}.

3. The component of the propeller thrust in the lift direction, A_T.

4. The lift due to the inclined tunnel flow on the propeller, A_L.

In general, the lift of the wing A_W by far exceeds the other components. Of the other three components, an important part with regard to the forces is played - except in extreme cases only - by that due to the propeller slipstream (A_{St}), while the other two (A_T and A_L) may be neglected. However, in the study of the moment equilibrium about the lateral axis, the two forces A_T and A_L are of significance since they generally act on a relatively large lever arm. Whereas the lift of the wing depends essentially on the angle of attack, in the case of

the other three components there also enters the effect of the angle κ since the propeller is attacked at the angle α - κ. For the normal range of values of α and κ the following may be stated. With increasing value of κ, A_{St} becomes larger since the angle at which the wing is attacked by the propeller slipstream becomes larger; A_T and A_L become smaller, however, since the angle between the propeller axis and the wind direction (= α - κ) becomes smaller.

Figures 51, 52, 53, and 54 show the increase in the lift slope $\frac{dc_a}{d\alpha}$ through the effect of the propeller. The effect described above - namely, that at smaller angles of attack the jet leads to a decrease in the lift - may also be observed in this case. The position of the point of intersection of the lift lines depends, however, on the angle κ, and the decrease in lift becomes less with decreasing κ. From the consideration on the lift distribution, it may be concluded that in the region of small angles of attack for larger values of κ, $A_{St} > A_T + A_L$. Furthermore, it is to be expected that at small values of λ that portion of the lift contributed directly by the propeller $(A_T + A_L)$ gains in importance and that with increasing κ, the total lift becomes smaller. Figure 55, showing the lift curves at λ = 0.13 for various values of κ, confirms this prediction.

Figure 56 shows $\frac{dc_a}{d\alpha}$ as a function of κ, and figure 57 as a function of λ. It may be seen that the effect of the angle κ on the total lift is not large. This fact comes out even more clearly when the polars are studied (figs. 58, 59, 60, and 61). Figure 62 shows the polars for λ = 0.13, 0.16, and 0.20 for various values of κ. With the exception of the polar for λ = 0.13 and κ = 9° the curves almost all coincide. This means therefore that in varying the angle κ within the prescribed limits, the individual effects (slipstream, inclined propeller, etc.) vary, but the sum of the effects on the entire wing-propeller system remains constant.

Except for the maximum lift region, in passing from one value of λ to another, the value of c_w changes by an amount which is independent of the lift coefficient (c_a); that is, for changes in λ the polars shift along the c_w axis. Starting from the polar of the wing alone, the value Δc_w by which c_w changes, is a measure of

$C_w = C_D$ in _____ _____

w _____ _____ which _____ _____

the propeller thrust. The disk loading of the propeller

$$c_s = \frac{S}{F_S \, q_0} \quad = \frac{8}{\pi} \, T_c \quad \text{where } T_c = \frac{thrust}{\rho V^2 D^2}$$

(S = thrust,

F_S = propeller disk area) $= \frac{\pi D^2}{4}$

$$c_s = \frac{T}{\pi \frac{D^2}{4} \frac{1}{2} \rho V^2} = \frac{8}{\pi} \frac{T}{\rho V^2 D^2}$$

is obtained from the relation:

$$c_s = \frac{F}{F_S} \, \Delta c_w \quad (F = \text{wing area})$$

Figure 63 shows c_s as a function of λ for the propel-
ler alone and for the propeller in the presence of the
wing.   The difference between the two curves gives the
interference effect of wing and propeller.

TABLE II

α	c_a	c_w	c_m
$-8°$	-0.102	0.012	0.044
$-6°$	$.040$	$.007$	$.089$
$-4°$	$.196$	$.010$	$.121$
$-2°$	$.351$	$.012$	$.164$
$0°$	$.502$	$.018$	$.195$
$2°$	$.661$	$.028$	$.240$
$4°$	$.816$	$.041$	$.285$
$6°$	$.965$	$.060$	$.320$
$8°$	1.104	$.078$	$.357$
$10°$	1.231	$.099$	$.394$
$12°$	1.342	$.119$	$.419$
$14°$	1.413	$.142$	$.452$
$16°$	1.434	$.168$	$.460$
$18°$	1.376	$.209$	$.478$

The moment curves (with respect to the wing leading edge) are shown in figures 64, 65, 66, and 67. The unstabilizing effect of the propeller may be seen first from the increase in the values of c_{mo}, and secondly, from the lowering in dc_m/dc_a with increasing values of λ. No effect of the angle κ on the values of dc_m/dc_a could be made out. (See fig. 68.) Figure 69 shows the variation of the stability coefficient dc_m/dc_a of the wing with propeller. Figure 70 shows the value $dc_m/d\lambda$, which plays an important part in the theory of longitudinal stability, as a function of λ. In the determination of these values, no dependence on c_a was found within the limits of accuracy employed.

For the determination of the lift distribution along the span, pressure-distribution measurements were carried out, the test set-up corresponding to the one already described. The measurements were made at the angles of attack which correspond to the main flight conditions: high-speed flight ($\alpha = -3^\circ$) and take-off and climb ($\alpha = 8^\circ$). The pressure-distribution curves are in this case not given since their character does not differ from the curves given in the preceding sections. Figures 71, 72, 73, and 74 show the spanwise lift distributions. For operating conditions, in which the propeller produces a thrust ($\lambda = 0.16$ and 0.20), the propeller slipstream gives rise to a strong increase in lift, whereas in the case where the propeller is operating as a windmill ($\lambda = 0.55$), the propeller slipstream results in a lowering of the lift. To the left sides of the figures the dynamic pressure increase and the angle of jet rotation act with opposite effect on the wing, and this explains the "unrest" in the lift distributions, particularly at the jet boundary ($y/R \approx -1$), where the vortices separating from the propeller-blade tips are located.

In the pressure-distribution measurements the value of $A_w + A_{St}$ is measured as the lift. The effect of the angle κ on the lift distribution must therefore be taken into account since A_{St} depends on κ, although A_w does not. This effect of κ may be clearly made out on the figures and is more evident in figure 75, which shows the lift distribution for $\lambda = 0.16$ with different values of κ. With increasing values of κ, the increase in lift as a result of the jet is greater since the direction of the jet causes an increase in the effective angle at the wing center.

Of particular importance is the separation process on attaining large angles of attack. In order to study this process, tuft investigations were made on the wing with and without propeller, and photographs also obtained on a film. Figure 76 presents the results of these tests. At the crosshatched areas the flow has separated. The left half of the figure shows how separation at the wing alone begins at the trailing edge of the wing center and from there on spreads over the entire wing. In the case of the wing in the presence of the propeller on the right half of the figure, the value of κ was 4° and $\lambda = 0.16$. Separation starts at the trailing edge at the positions of the jet boundary, and from there on the separation is propagated toward the wing tips, whereas in the jet region itself the flow continues to adhere far beyond the maximum lift. No effect of the nonsymmetry due to the propeller rotation could clearly be made out on the separation process.

Downwash Measurements

In a plane $2\frac{1}{2}$ chords behind the wing leading edge, the downwash was measured in direction and magnitude with the aid of a dynamic pressure sphere. The test set-up is shown on figure 77, and figure 78 shows the relative dimensions. The measurements were made along two horizontal lines: one in the projection of the wing chord (position I), the other 0.29 chord above the latter (position II). In changing the angle of attack of the wing the position of the sphere was likewise always changed to correspond to the rigid arrangement of wing and tail.

The moment M_H of a horizontal tail surface is, with the usual notation

$$M_H = q_0 \; F_H \; l \; c'_{n_H} \; (\alpha - \delta) \; \frac{q_H}{q_0}$$

and hence the stability contribution of the tail

$$\frac{\partial M_H}{\partial \alpha} = q_0 \; F_H \; l \; c'_{n_H} \left[\frac{\partial}{\partial \alpha} \frac{(\alpha - \delta) \; q_H}{q_0} \right]$$

The factors in front of the brackets are design values of the tail while the expression within the brackets is a measure of the quality of the flow at the position of the tail. This value we shall denote by ϵ. It is immediately evident that for an elevator in a nondisturbed flow

$\epsilon = 1$. The terms elsewhere proposed of "tail efficiency" or "stability efficiency" do not correctly bring out the significance of ϵ; a better term would appear to be "efficiency of the tail flow." Therefore, we have:

$$\epsilon = \frac{\partial\,(\alpha - \delta)}{\partial\alpha}\,\frac{q_H}{q_0} + \frac{\partial\,\frac{q_H}{q_0}}{\partial\alpha}\,(\alpha - \delta)$$

In our measurements, in which λ and q_0 were held constant with change in angle of attack,

$$\frac{\partial\,\frac{q_H}{q_0}}{\partial\,\alpha}$$

may approximately be set equal to zero, so that

$$\epsilon = \left(1 - \frac{\partial\delta}{\partial\alpha}\right)\frac{q_H}{q_0}$$

Figure 79 shows the downwash for the wing without propeller. At the angle of attack $\alpha = 16°$, the flow had already separated. The small downwash value at $\alpha = 8°$ arises from the fact that in this case the sphere was located in the dead-air region of the wing. The effect of the propeller on the downwash relations is shown on figures 80, 81, 82, and 83. The crosshatched areas give the changes in the dynamic pressure. The values shown are for $\alpha = -3°$ and $8°$. In order to include the effect of the inclination of the propeller to the wing chord the measurements were taken for $\kappa = 9°$ and $-6°$.

In the study of the downwash, it is to be noted that several factors determine the flow behind the wing with propeller, namely, the downwash of the wing itself, the dead-air region of the wing, the locally limited propeller slipstream with rotation and variation in dynamic pressure, and the effect of the slipstream on the flow in its neighborhood. According to the angle of attack the propeller slipstream will envelop the entire tail or only a part of it, or may pass above or below it. The dead-air region of the wing leads in general to a decrease in the downwash and the dynamic pressure. The shape of the dead-air region is changed by the jet. Figures 80 to 83 show the interaction of all these factors. In position I (in the projection of the wing chord) the jet effect may be

made out in the case of all four measurements, whereas in
position II, particularly at α = -3°, the direct jet ef-
fect is vanishingly small. The upper half of figure 80
brings out the effect of the dead-air region of the wing.
Figures 84 and 85 show the variation of ε, the "efficien-
cy of the tail flow" along the span. Difficulties were met
with in determining ∂δ/∂α since the value of δ very
much depends on which of the many factors mentioned above
is predominant at the particular position. It is impossi-
ble to make any definite statement as to whether the sta-
bility contribution of a tail surface in the flow investi-
gated is diminished by the effect of the propeller slip-
stream. In all the measurements it may clearly be made
out that there exists upwash near the jet. The inclina-
tion of the propeller axis (κ) has no demonstrable ef-
fect on the downwash, which fact is in good agreement with
the constancy found for the total lift.

VI. SUMMARY

In the first part of the investigation the effect on
a wing of a jet without rotation with constant velocity
distribution, is determined. The jet gives rise to an in-
crease in the lift. No accurate check on the theory of
Koning, which underlies this case, could be undertaken
since some of the assumptions made in the theory cannot be
satisfied in the test. The downwash measurements at the
tail location showed an increase in the downwash angle due
to the jet.

In the second part of the investigation the wing was
under the effect of the jet from a propeller whose axis
was fixed in the direction of the undisturbed wind. The
rotation and the dynamic pressure changes in the jet re-
sult in a nonsymmetrical variation in the lift. Study of
the downwash relations led to the result that the two por-
tions into which the jet is divided by the wing do not
again reunite behind the wing but that each portion experi-
ences a lateral deviation in the direction of the jet ro-
tation.

In the third part, the mutual interaction of wing and
propeller was investigated. The propeller shaft, which
was driven by a motor attached outside the wing itself,
could be inclined with respect to the wing chord. This
inclination has considerable effect on the change in lift
of the wing by the propeller slipstream. The total lift of

the wing-propeller system in which lift is included besides that of the wing proper, the component of the propeller thrust in the lift direction and the lift due to the inclined position of the propeller with respect to the wind direction, is hardly affected by the inclination of the propeller to the wing chord, and similarly, no effect could be established on the moment curve. The propeller increases the instability of the wing. By downwash measurements it was determined to what extent the character of the flow at the tail is changed under the effect of the propeller slipstream.

Translation by S. Reiss,
National Advisory Committee
for Aeronautics.

REFERENCES AND BIBLIOGRAPHY

1.   Blenk, H.: Flight Tests for the Determination of
        Static Longitudinal Stability. T.M. No. 584,
        N.A.C.A., 1930.

2.   Blenk, H.: Luftschraubenstrahl und Längsstabilität.
        Luftfahrtforschung, vol. 11, 1935, p. 202.

3.   Blenk, H., and Fuchs, D.: Druckmessungen an einem
        durch einen Luftstrahl hindurchgesteckten Trag-
        flugel. DVL Jahruch, 1931.

4.   Bradfield, F. B.: Preliminary Tests on the Effect on
        the Lift of aWing of the Position of the Airscrews
        Relative to It. R. & M. No. 1212, British A.R.C.,
        1928.

5.   Bradfield, F. B.: Wind Tunnel Data on the Effect of
        Slipstream on the Downwash and Velocity at the
        Tailplane. R. & M. No. 1488, British A.R.C., 1932.

6.   Ebert, H.: Über Flugversuche zur Messung der Flug-
        zeugpolare und den Einfluss des Schraubenstrahls.
        DVL Jahrbuch, 1932.

7.   Ferrari, C.: Über den Einfluss der Luftschraube auf
        die aerodynamischen Eigenschaften des Flügels.
        L'Aerotecnica, vol. 13, 1933.

8. Flachsbart, O., and Kröber, G.: Experimental Inves-
        tigation of Aircraft Propellers Exposed to Ob-
        lique Air Currents. T.M. No. 562, N.A.C.A., 1930.

9. Gorski, V. P.: Untersuchung über den Einfluss des
        Rumpfes und der Tragfläche auf horizontale Schwanz-
        flächen des Flugzeugs. CAHI Report 131, 1932.

10. Glauert, H.: The Lift and Drag of a Wing Spanning a
        Free Jet. R. & M. No. 1603, British A.R.C., 1934.

11. Hübner, W.: Messung der Höhensteuerkräfte und der
        Längsstabilität eines Flugzeugs vom Muster Junkers
        F 13 ge. DVL Jahrbuch, 1930.

12. Hübner, W.: Ergebnisse von Messungen der Stabilität
        um die Querachse. DVL Jahrbuch, 1931, p. 684.

13. Hübner, W.: Ergebnisse von Messungen der statischen
        Längsstabilität einiger Flugzeuge. DVL Jahrbuch,
        1933.

14. Koning, C.: Influence of the Propeller on the Other
        Parts of the Airplane Structure. Durand, Aero-
        dynamic Theory, vol. 4, 1935.

15. Millikan, C. B., Russell, J. S., and McCoy, H. M.:
        Wind Tunnel Tests on a High Wing Monoplane. Jour.
        of the Aeronautical Sciences, vol. 3, no. 3, 1936.

16. Misztal, F.: Zur Frage der schräg angeblasenen Pro-
        peller. Abh. aus dem Aerod. Inst. Aachen, no. 11,
        1929.

17. Ostoslavsky, I., and Halesoff, D.: Interference be-
        tween Airscrew and Aeroplane. CAHI Report 213,
        1935.

18. Pistolesi, E.: Sull'ala traversante un getto libero;
        Atti della Pontificia Academia delle Scienze,
        Nuovo Lincei, vol. 86, 1933.

19. Pistolesi, E.: L'influsso della limitazione delle
        corrente sulle cratteristiche dei modolli di ali.
        L'Aerotecnica, vol. 16, 1936.

20. Pleines, W.: Flugmessungen im Höchstauftriebsbereich
        mit dem Flugzeug Focke-Wulf A 32 "Buzzard".
        Luftfahrtforschung, vol. 12, July 30, 1935, p. 142.

21. Prandtl, L.: Tragflügeltheorie. Neudruck, Vier Ab-
     handlungen zur Hydrodynamik und Aerodynamik von
     L. Prandtl und A. Betz. Göttingen, 1927.

22. Robinson, R. G., and Herrnstein, W. H.: Wing-Nacelle-
     Propeller Interference for Wings of Various Spans.
     Force and Pressure-Distribution Tests. T.R. No.
     569, N.A.C.A., 1936.

23. Stüper, J.: An Airfoil Spanning an Open Jet. T.M.
     No. 723, N.A.C.A., 1933.

24. Stüper, J.: Contribution to the Problem of Airfoils
     Spanning a Free Jet. T.M. No. 796, N.A.C.A., 1936.

25. Wood, D. H., McHugh, J. G., Valentine, E. F., and
     Bioletti, C.: Tests of Nacelle-Propeller Combina-
     tions in Various Positions with Reference to Wings.

     Part   I - Thick Wing - N.A.C.A. Cowled Nacelle -
               Tractor Propeller, by D. H. Wood.
               T.R. No. 415, N.A.C.A., 1932.

     Part II - Thick Wing - Various Radial-Engine Cowl-
               ings - Tractor Propeller, by D. H.
               Wood. T.R. No. 436, N.A.C.A., 1932.

     Part III - Clark Y Wing - Various Radial-Engine
               Cowlings - Tractor Propeller, by D.
               H. Wood. T.R. No. 462, N.A.C.A., 1933.

     Part IV - Thick Wing - Various Radial-Engine Cowl-
               ings - Tandem Propellers, by J. G.
               McHugh. T.R. No. 505, N.A.C.A., 1934.

     Part   V - Clark Y Biplane Cellule - N.A.C.A.
               Cowled Nacelle - Tractor Propeller,
               by E. F. Valentine. T.R. No. 506,
               N.A.C.A., 1934.

     Part VI - Wings and Nacelles with Pusher Propel-
               ler, by D. H. Wood and C. Bioletti.
               T.R. No. 507, N.A.C.A., 1934.

26. Lotz, I.: Einfluss des Schraubenstrahls auf die Auf-
     triebsverteilung. Jahrbuch, 1936, der Lilienthal-
     Gesellschaft. Verlag von R. Oldenbourg, München
     und Berlin.

Table 3.

	a	$K=9°$			$K=4°$			$K=-1°$			$K=-6°$		
		c_a	c_w	c_m	c_a	c_w	c_m	c_a	c_w	c_m	c_a	c_w	c_m
$\lambda=0,13$	$-8°$	$-0,247$	$-0,441$	$0,101$	$-0,211$	$-0,418$	$0,104$	$-0,192$	$-0,420$	$0,123$	$-0,154$	$-0,425$	$0,132$
	$-4°$	$0,146$	$-0,450$	$0,183$	$0,178$	$-0,427$	$0,184$	$0,210$	$-0,433$	$0,199$	$0,244$	$-0,430$	$0,203$
	$0°$	$0,530$	$-0,443$	$0,251$	$0,561$	$-0,411$	$0,252$	$0,591$	$-0,421$	$0,262$	$0,639$	$-0,416$	$0,270$
	$4°$	$0,909$	$-0,418$	$0,325$	$0,955$	$-0,374$	$0,331$	$0,968$	$-0,376$	$0,345$	$1,030$	$-0,372$	$0,352$
	$8°$	$1,293$	$-0,364$	$0,399$	$1,316$	$-0,324$	$0,422$	$1,335$	$-0,319$	$0,425$	$1,376$	$-0,306$	$0,432$
	$12°$	$1,621$	$-0,296$	$0,483$	$1,645$	$-0,271$	$0,480$	$1,672$	$-0,259$	$0,485$	$1,696$	$-0,221$	$0,502$
	$16°$	$1,831$	$-0,224$	$0,531$	$1,848$	$-0,183$	$0,545$	$1,860$	$-0,165$	$0,545$	$1,880$	$-0,138$	$0,560$
	$18°$	$1,803$	$-0,143$	$0,535$	$1,815$	$-0,130$	$0,575$	$1,820$	$-0,107$	$0,586$	$1,843$	$-0,070$	$0,592$
$\lambda=0,16$	$-8°$	$-0,195$	$-0,247$	$0,079$	$-0,167$	$-0,249$	$0,088$	$-0,148$	$-0,257$	$0,102$	$-0,133$	$-0,258$	$0,093$
	$-4°$	$0,174$	$-0,251$	$0,167$	$0,191$	$-0,254$	$0,155$	$0,202$	$-0,258$	$0,163$	$0,236$	$-0,258$	$0,171$
	$0°$	$0,526$	$-0,241$	$0,233$	$0,542$	$-0,237$	$0,234$	$0,554$	$-0,240$	$0,236$	$0,586$	$-0,241$	$0,239$
	$4°$	$0,899$	$-0,213$	$0,316$	$0,904$	$-0,212$	$0,311$	$0,922$	$-0,206$	$0,320$	$0,947$	$-0,209$	$0,317$
	$8°$	$1,236$	$-0,163$	$0,387$	$1,236$	$-0,170$	$0,386$	$1,270$	$-0,166$	$0,396$	$1,286$	$-0,153$	$0,390$
	$12°$	$1,536$	$-0,104$	$0,465$	$1,536$	$-0,106$	$0,449$	$1,561$	$-0,101$	$0,468$	$1,584$	$-0,091$	$0,467$
	$16°$	$1,715$	$-0,045$	$0,515$	$1,708$	$-0,035$	$0,490$	$1,711$	$-0,022$	$0,519$	$1,736$	$0,012$	$0,522$
	$18°$	$1,651$	$0,003$	$0,522$	$1,664$	$0,008$	$0,529$	$1,660$	$0,023$	$0,526$	$1,700$	$0,030$	$0,540$
$\lambda=0,20$	$-8°$	$-0,165$	$-0,129$	$0,067$	$-0,147$	$-0,132$	$0,072$	$-0,128$	$-0,135$	$0,077$	$-0,125$	$-0,141$	$0,071$
	$-4°$	$0,183$	$-0,134$	$0,149$	$0,195$	$-0,131$	$0,149$	$0,198$	$-0,135$	$0,145$	$0,220$	$-0,138$	$0,149$
	$0°$	$0,522$	$-0,120$	$0,225$	$0,526$	$-0,117$	$0,220$	$0,530$	$-0,120$	$0,216$	$0,551$	$-0,121$	$0,237$
	$4°$	$0,862$	$-0,095$	$0,302$	$0,868$	$-0,086$	$0,299$	$0,886$	$-0,092$	$0,309$	$0,895$	$-0,093$	$0,299$
	$8°$	$1,184$	$-0,049$	$0,386$	$1,183$	$-0,047$	$0,369$	$1,207$	$-0,048$	$0,378$	$1,215$	$-0,044$	$0,383$
	$12°$	$1,487$	$0,010$	$0,456$	$1,470$	$0,001$	$0,436$	$1,486$	$0,003$	$0,447$	$1,501$	$0,010$	$0,447$
	$16°$	$1,628$	$0,058$	$0,501$	$1,620$	$0,063$	$0,485$	$1,620$	$0,071$	$0,496$	$1,632$	$0,075$	$0,498$
	$18°$	$1,552$	$0,110$	$0,511$	$1,561$	$0,107$	$0,513$	$1,568$	$0,111$	$0,504$	$1,567$	$0,117$	$0,501$
$\lambda=0,35$	$-8°$	$-0,118$	$0,011$	$0,054$	$-0,114$	$0,015$	$0,051$	$-0,102$	$0,013$	$0,050$	$-0,113$	$0,013$	$0,041$
	$-4°$	$0,195$	$0,008$	$0,130$	$0,196$	$0,012$	$0,128$	$0,188$	$0,014$	$0,119$	$0,196$	$0,013$	$0,119$
	$0°$	$0,483$	$0,021$	$0,193$	$0,489$	$0,028$	$0,096$	$0,491$	$0,024$	$0,188$	$0,495$	$0,025$	$0,187$
	$4°$	$0,810$	$0,050$	$0,278$	$0,801$	$0,051$	$0,273$	$0,803$	$0,051$	$0,270$	$0,809$	$0,049$	$0,268$
	$8°$	$1,100$	$0,092$	$0,355$	$1,092$	$0,087$	$0,339$	$1,102$	$0,087$	$0,343$	$1,098$	$0,087$	$0,342$
	$12°$	$1,351$	$0,128$	$0,419$	$1,344$	$0,126$	$0,402$	$1,348$	$0,129$	$0,411$	$1,357$	$0,131$	$0,417$
	$16°$	$1,496$	$0,172$	$0,467$	$1,480$	$0,175$	$0,454$	$1,478$	$0,181$	$0,451$	$1,488$	$0,181$	$0,460$
	$18°$	$1,441$	$0,224$	$0,487$	$1,410$	$0,209$	$0,486$	$1,429$	$0,214$	$0,464$	$1,426$	$0,209$	$0,465$
$\lambda=0,55$	$-8°$	$-0,109$	$0,035$	$0,047$	$-0,108$	$0,037$	$0,042$	$-0,098$	$0,037$	$0,044$	$-0,112$	$0,040$	$0,035$
	$-4°$	$0,194$	$0,030$	$0,123$	$0,192$	$0,034$	$0,120$	$0,186$	$0,035$	$0,114$	$0,190$	$0,036$	$0,114$
	$0°$	$0,490$	$0,044$	$0,189$	$0,480$	$0,048$	$0,190$	$0,480$	$0,048$	$0,185$	$0,482$	$0,050$	$0,183$
	$4°$	$0,797$	$0,070$	$0,270$	$0,787$	$0,070$	$0,268$	$0,787$	$0,073$	$0,268$	$0,784$	$0,071$	$0,263$
	$8°$	$1,079$	$0,107$	$0,351$	$1,064$	$0,105$	$0,337$	$1,076$	$0,108$	$0,341$	$1,058$	$0,108$	$0,337$
	$12°$	$1,314$	$0,148$	$0,412$	$1,306$	$0,145$	$0,392$	$1,305$	$0,148$	$0,412$	$1,313$	$0,149$	$0,403$
	$16°$	$1,424$	$0,206$	$0,470$	$1,428$	$0,199$	$0,469$	$1,450$	$0,199$	$0,458$	$1,455$	$0,200$	$0,458$
	$18°$	$1,392$	$0,251$	$0,464$	$1,395$	$0,222$	$0,484$	$1,422$	$0,220$	$0,462$	$1,419$	$0,222$	$0,468$
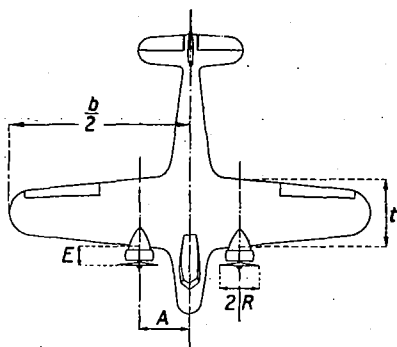
Table 3

Figure 1.–Notation of dimensions for table I.

Figure 7.–Polars of the wing with and without blower.

Figure 6.–Lift coefficient as a function of the angle of attack.
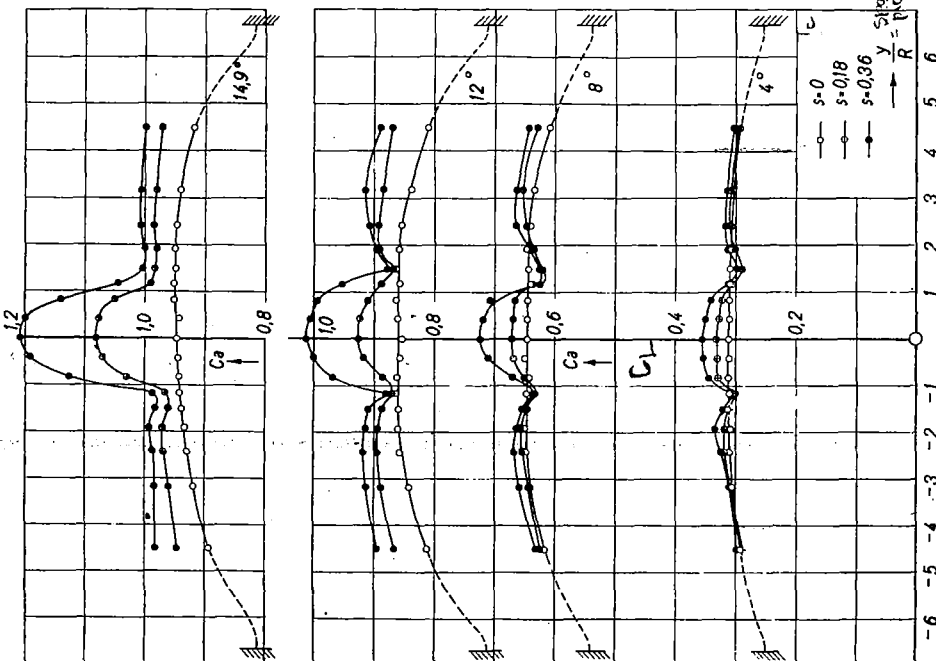
Figure 13.–Spanwise lift distribution.

$A = $ Slipstream velocity increment

$$\lambda = -1 + \sqrt{1 + \frac{8}{\pi} \frac{T_c}{R}}$$
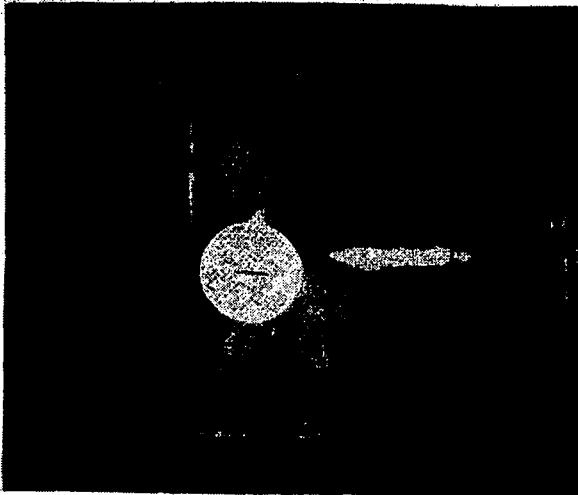
Figure 2.- Test set-up for measur-
ing the polars.
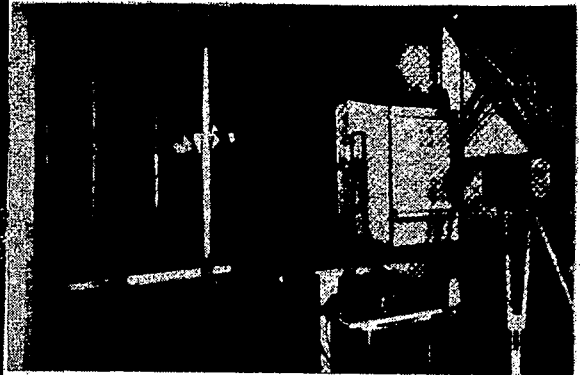
Figure 8.- Test set-up for the
pressure distribu-
tion measurements.

Figure 19.- Test-up for the down-
wash measurements with
a feoler vane.
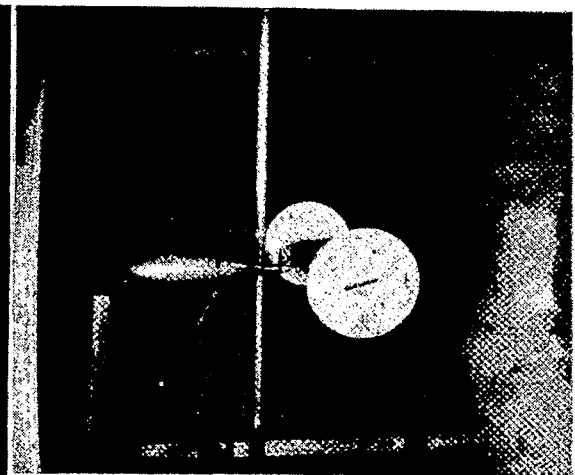
Figure 22.- Wing in propeller slip-
stream.
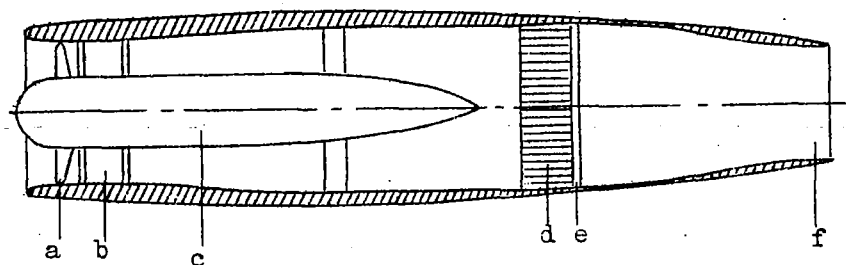
Figure 3.- Cross section of fan and casing.
a propeller, b guide vanes, c motor, d honeycomb, e mesh, f throat.

Figure 5.- Dynamic pressure distribution in jet, s = 0.36.
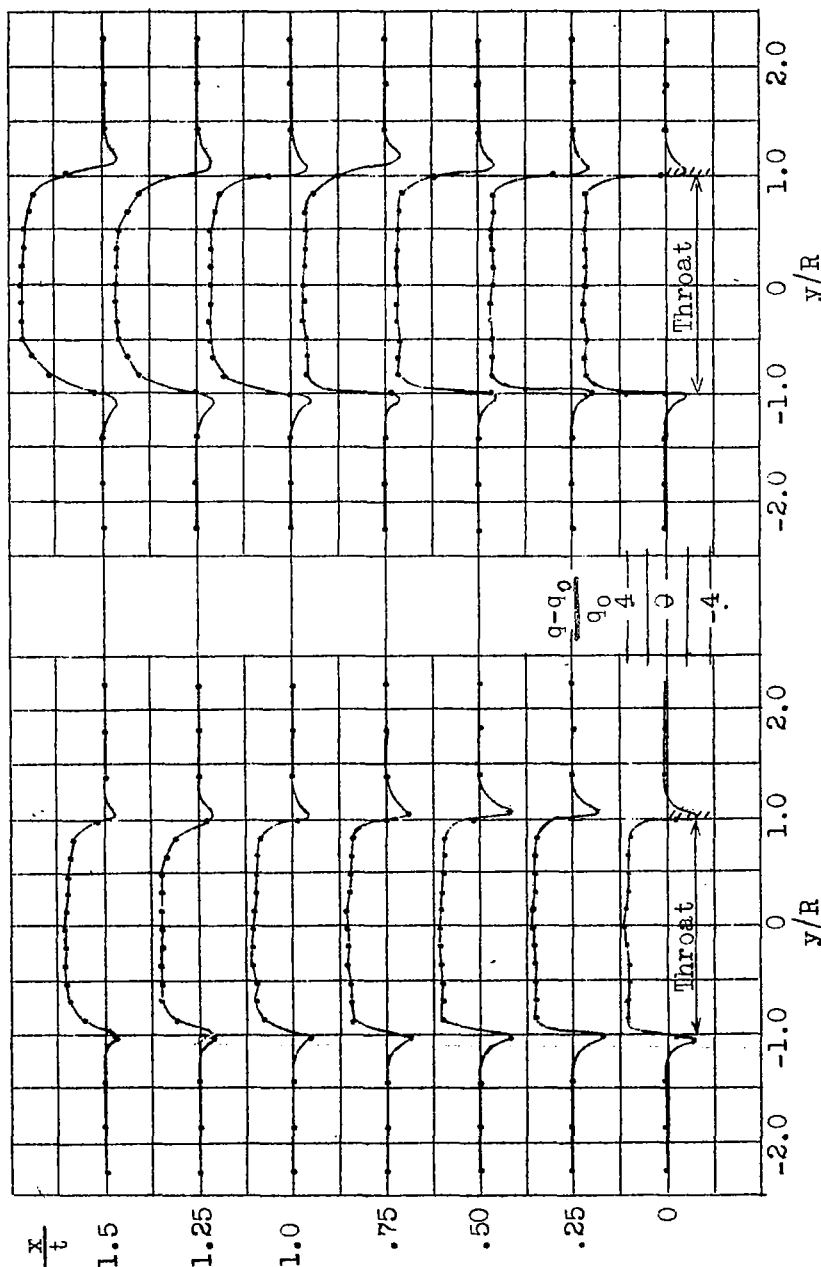
Figure 4.- Dynamic pressure distribution in jet, s = 0.18.

Figure 9. α = 4°
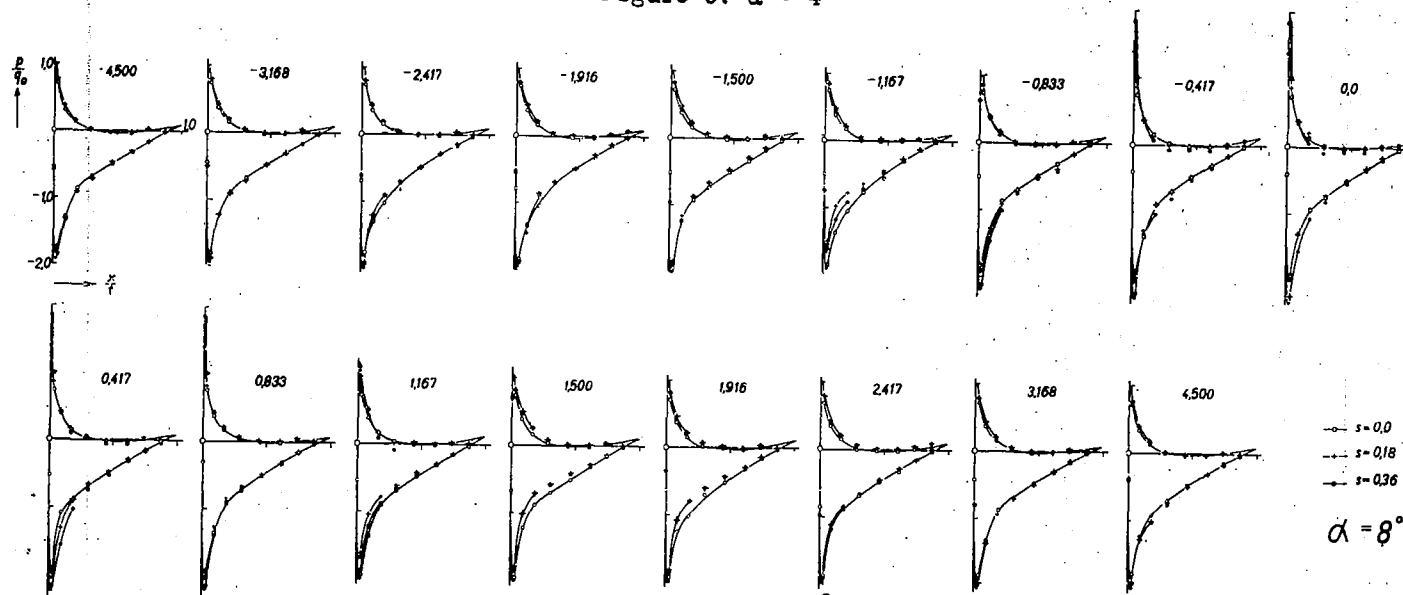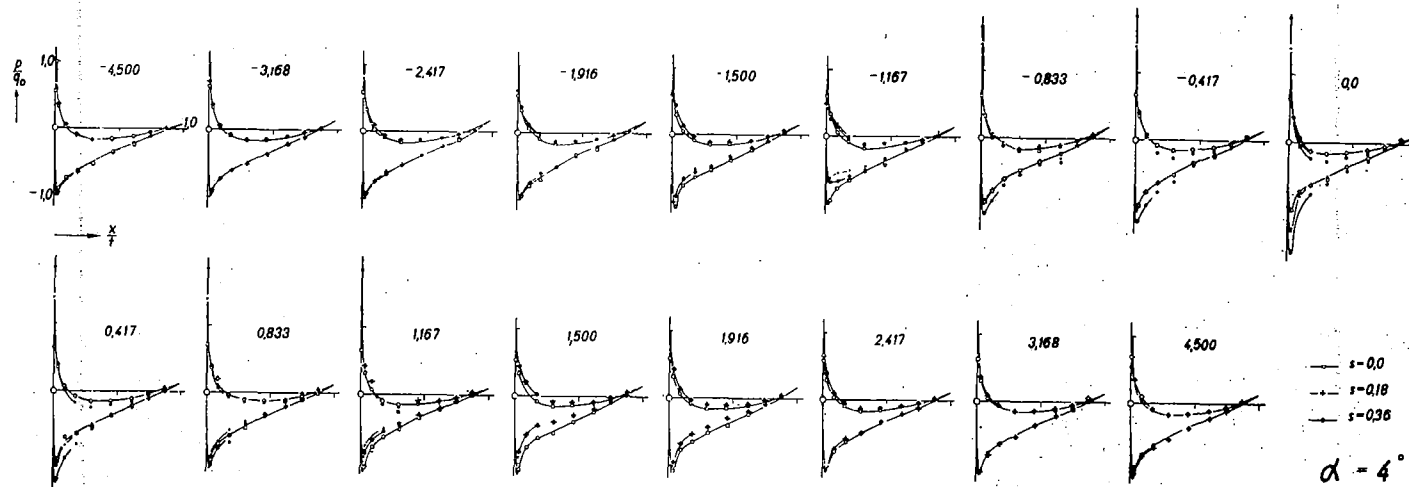
Figure 10. α = 8°
Chordwise pressure distributions.

WITH JET
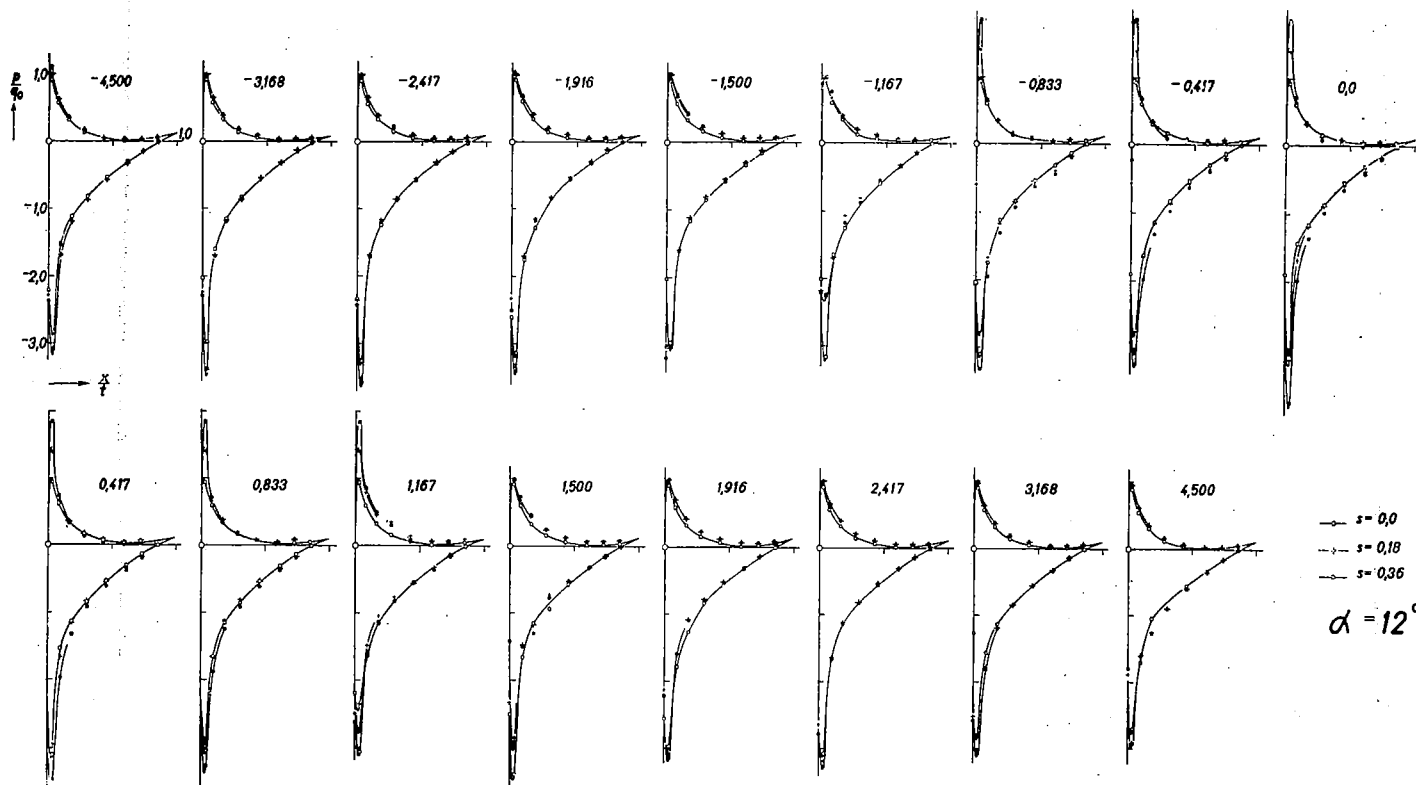
Figure 11.-Chordwise pressure distributions. α = 12°.

Fig.11

Figure 12.-Chordwise pressure distributions. $\alpha = 14.9^{\circ}$.

Fig. 12
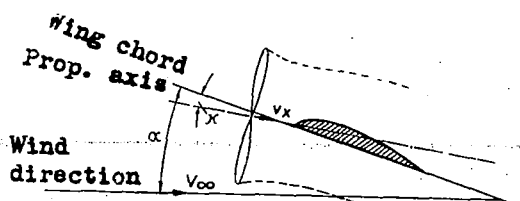
Figure 14.- Increase in lift according to the theory. Position of wing with respect to the propeller and the relative wind direction.

Figure 15.- Lift distribution according to theory and measurement, s = 0.18.

Figure 18.- Increase in lift according to measurements.
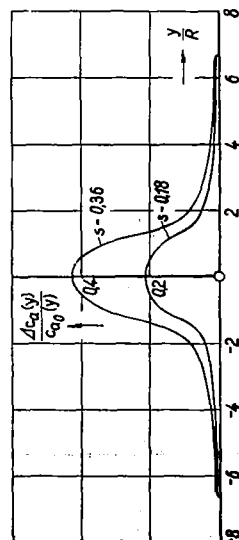
Figure 17.- Increase in lift according to the theory.

---- Computed by Lotz {Wing alone
  o   Measured
---- Computed by Koning}
  •   Measured} Wing with jet.

Figure 16.- Lift distribution according to theory and measurement s = 0.36.
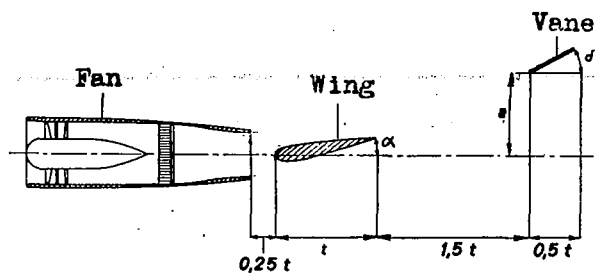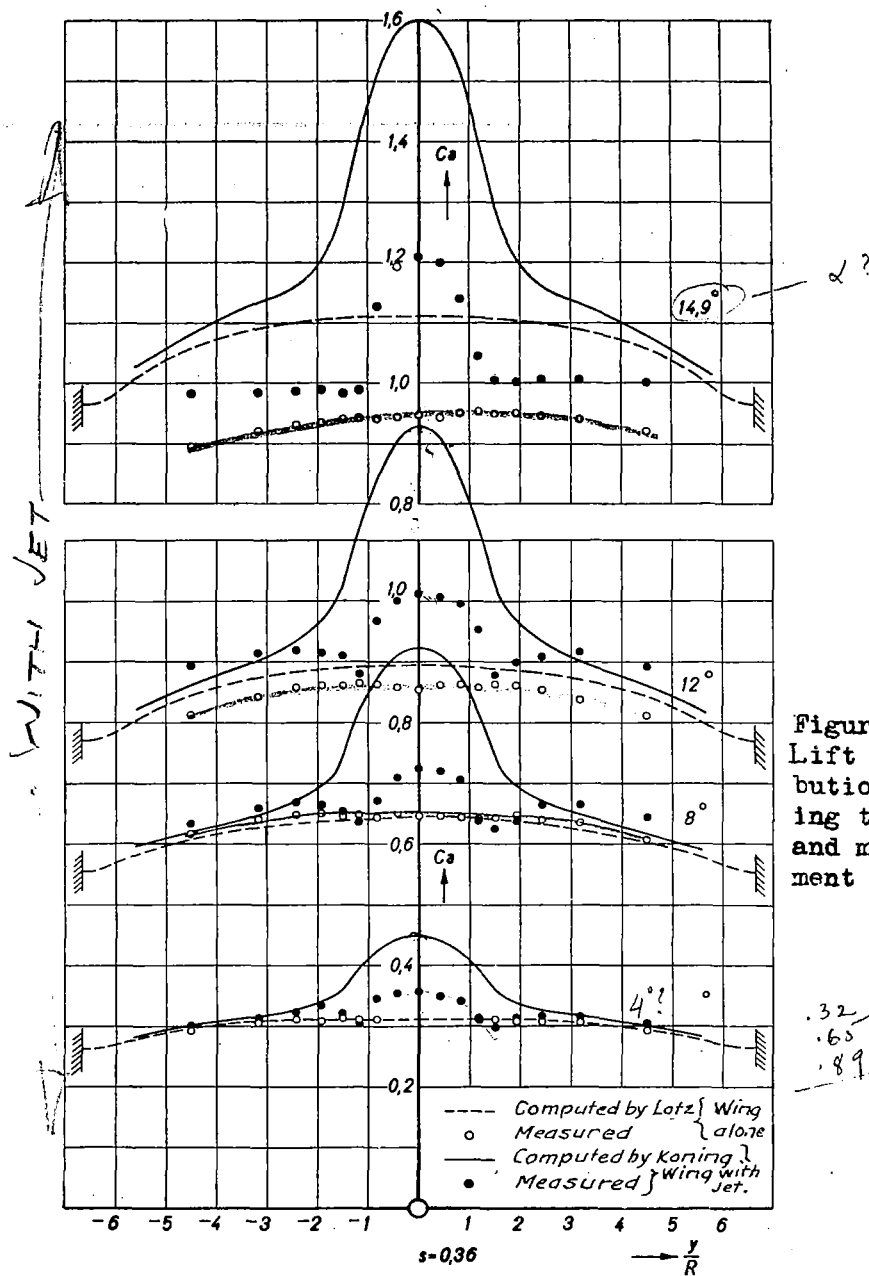
Figure 20.- Arrangement for the downwash measurements.
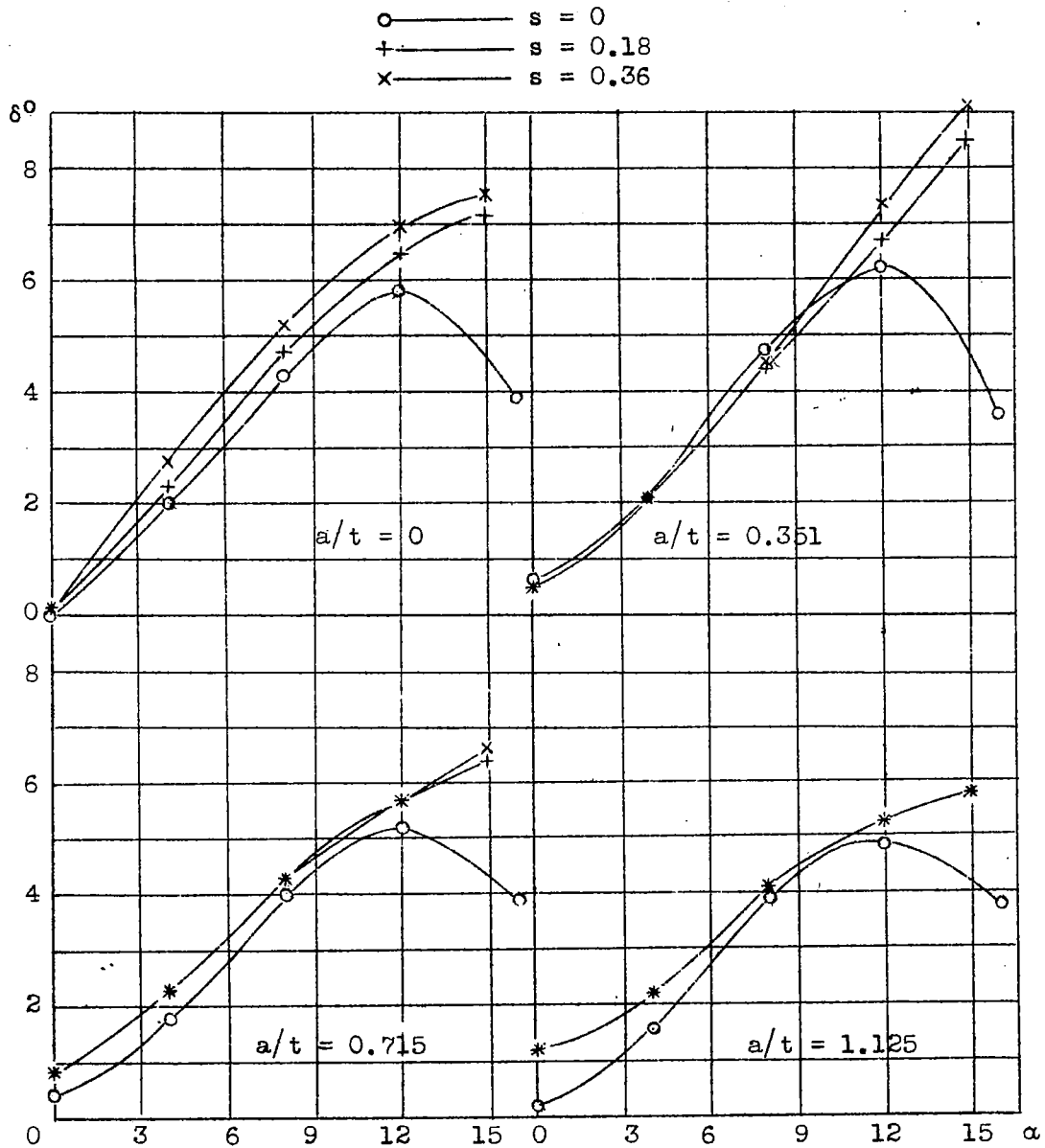
Figure 21.- Variation of the downwash angles.
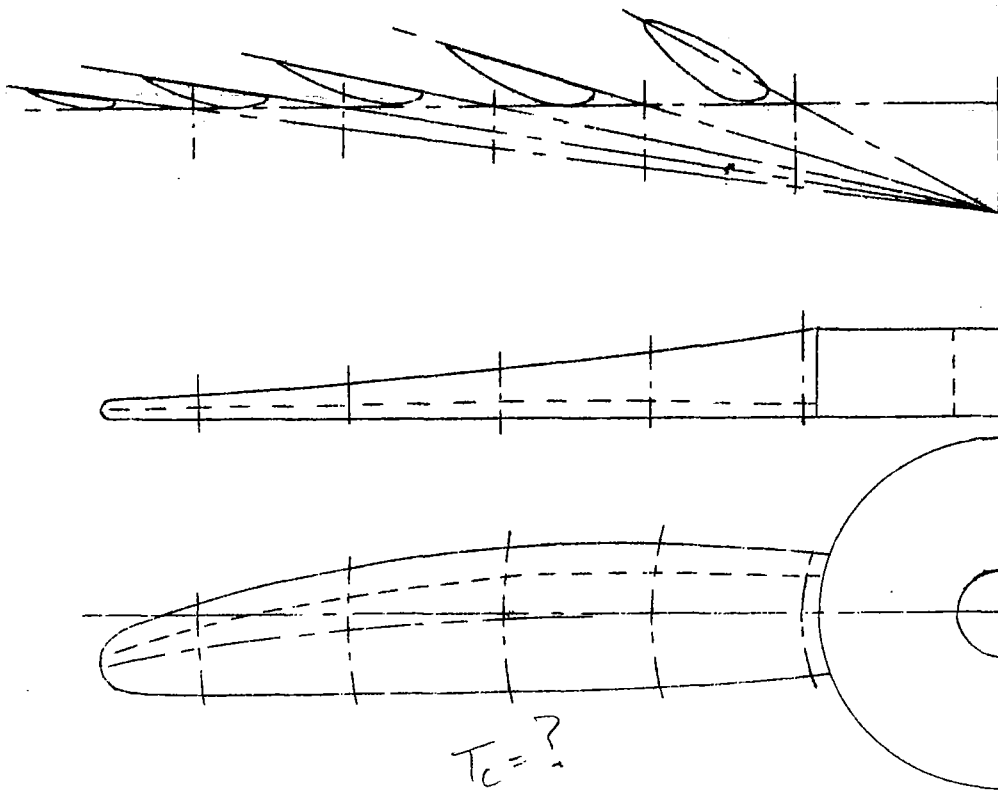
Figure 23.- Dimensioning of propeller. (American notation S_1, F_2, A_1, 0.4)

$T_c = ?$
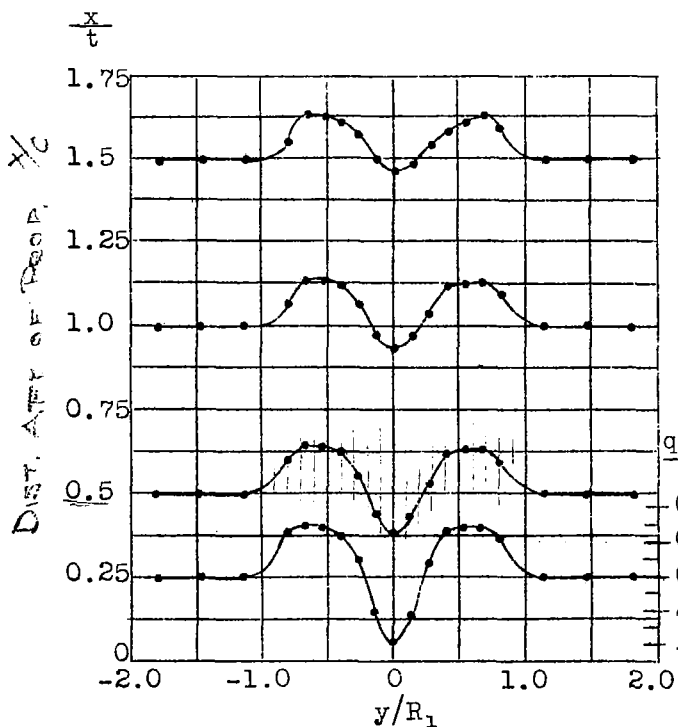
Figure 25.- Spanwise distribution of dynamic pressure in propeller slipstream.
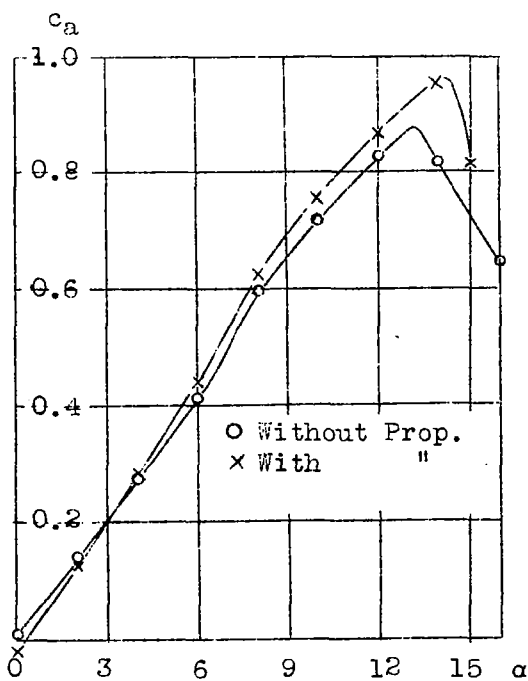
o Without Prop.
× With   "

Figure 26.- Wing lift in propeller slipstream.
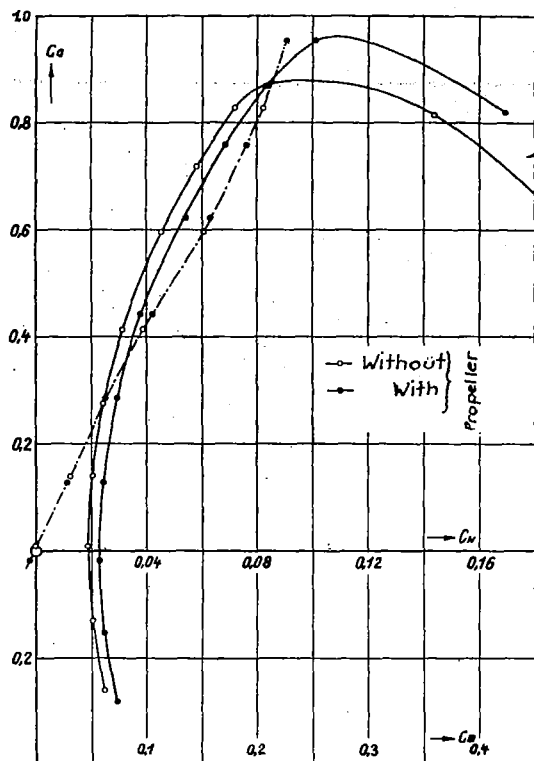
Figure 27.- Polar with and without propeller slipstream.

Figure 24.- Spanwise variation of jet rotation angle in propeller slipstream.
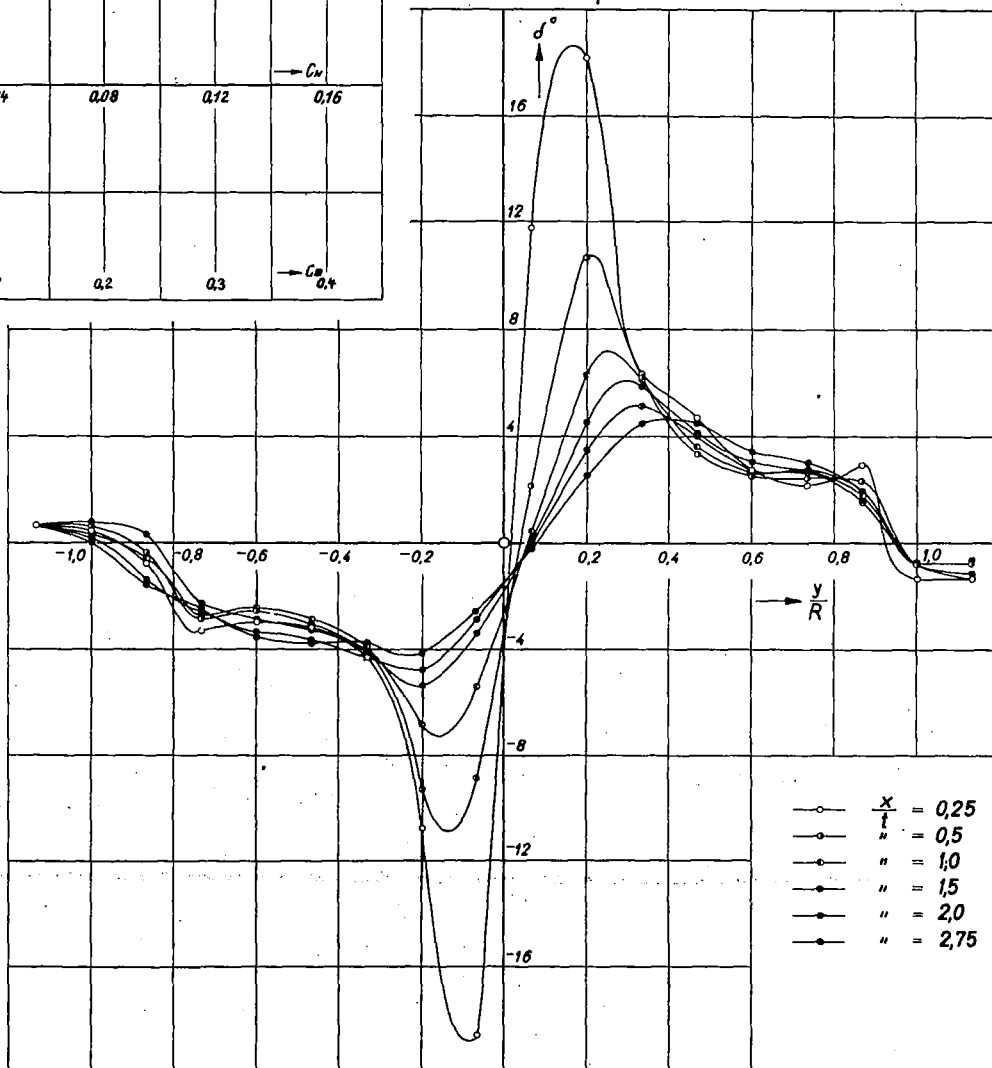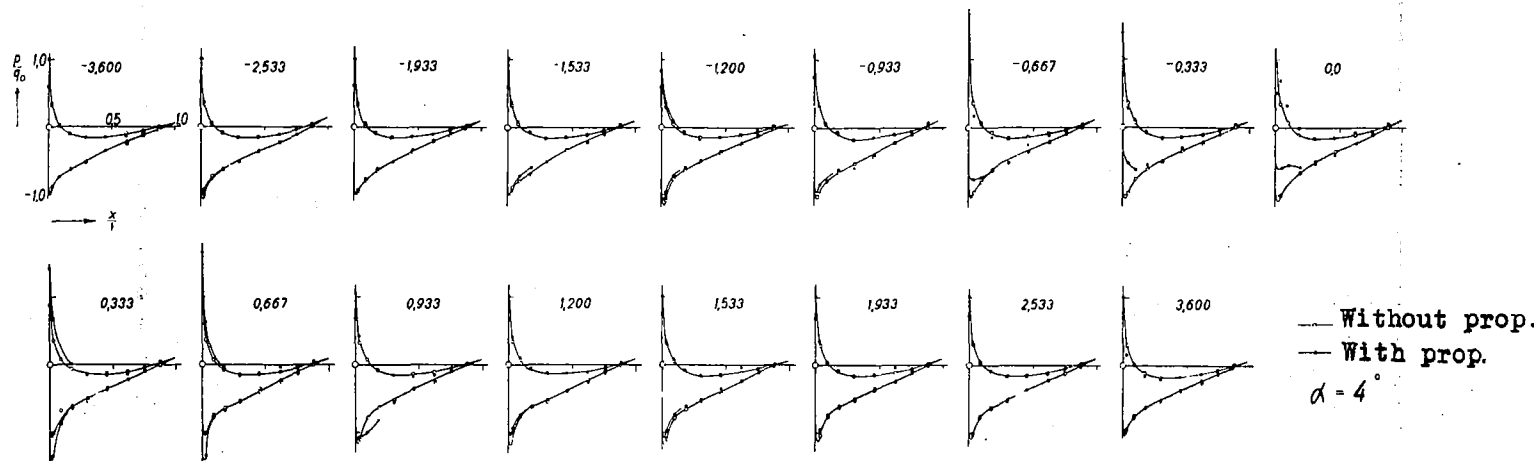
Figure 28.- Chordwise pressure distribution, $\alpha = 4^\circ$
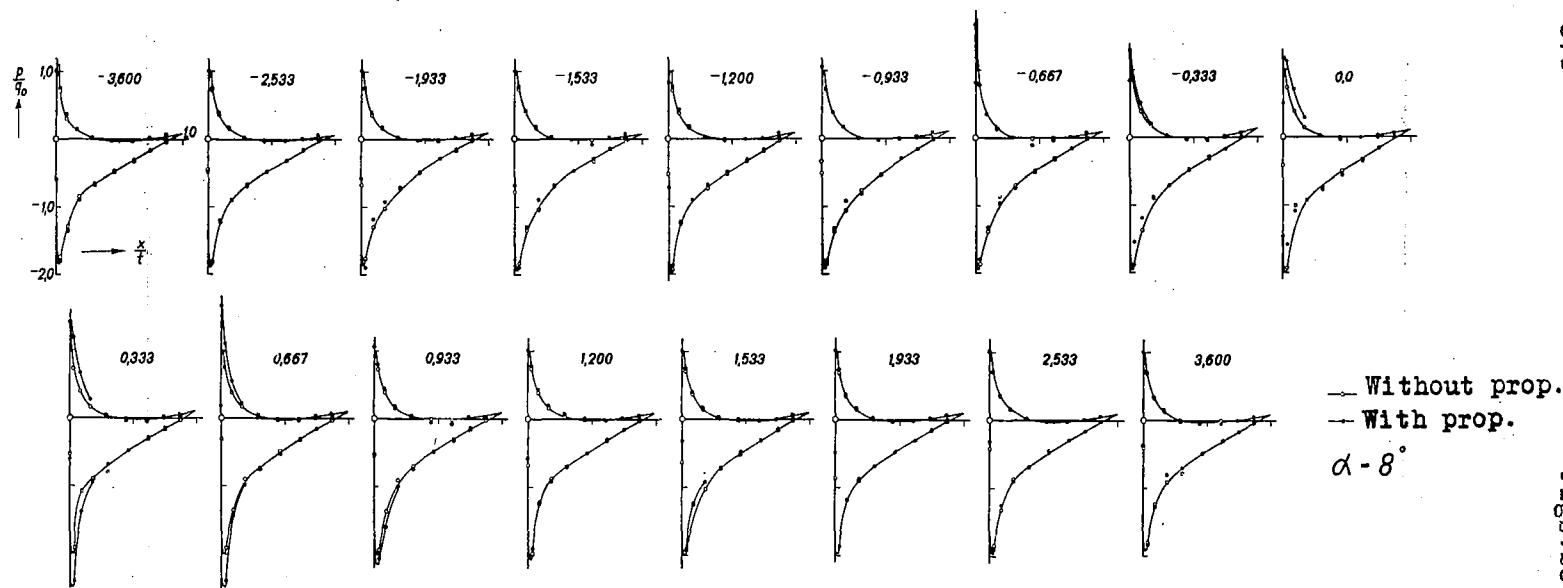
Figure 29.- Chordwise pressure distribution, $\alpha = 8^\circ$

WITH PROP.
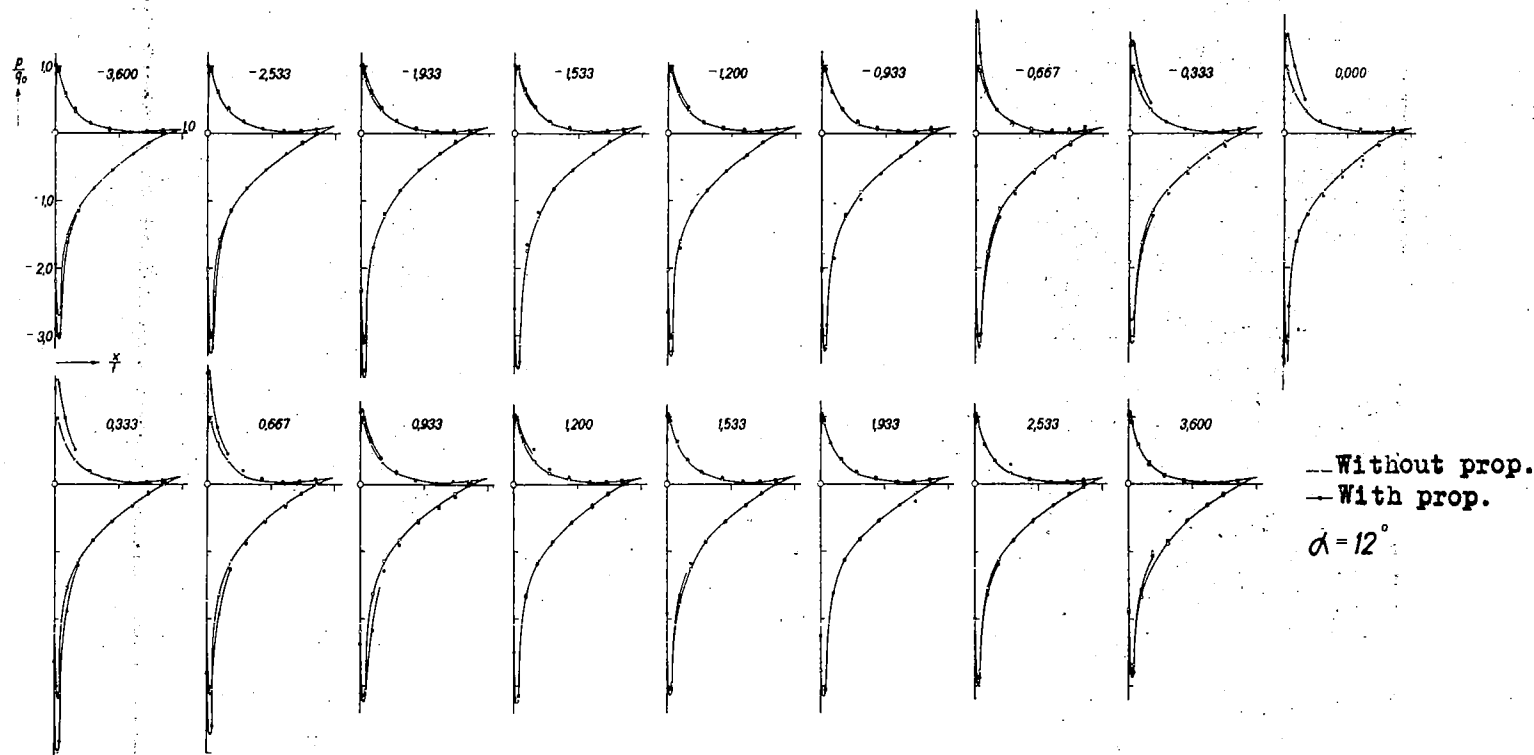
Figure 30.- Chordwise pressure distribution, α = 12°

Fig. 30
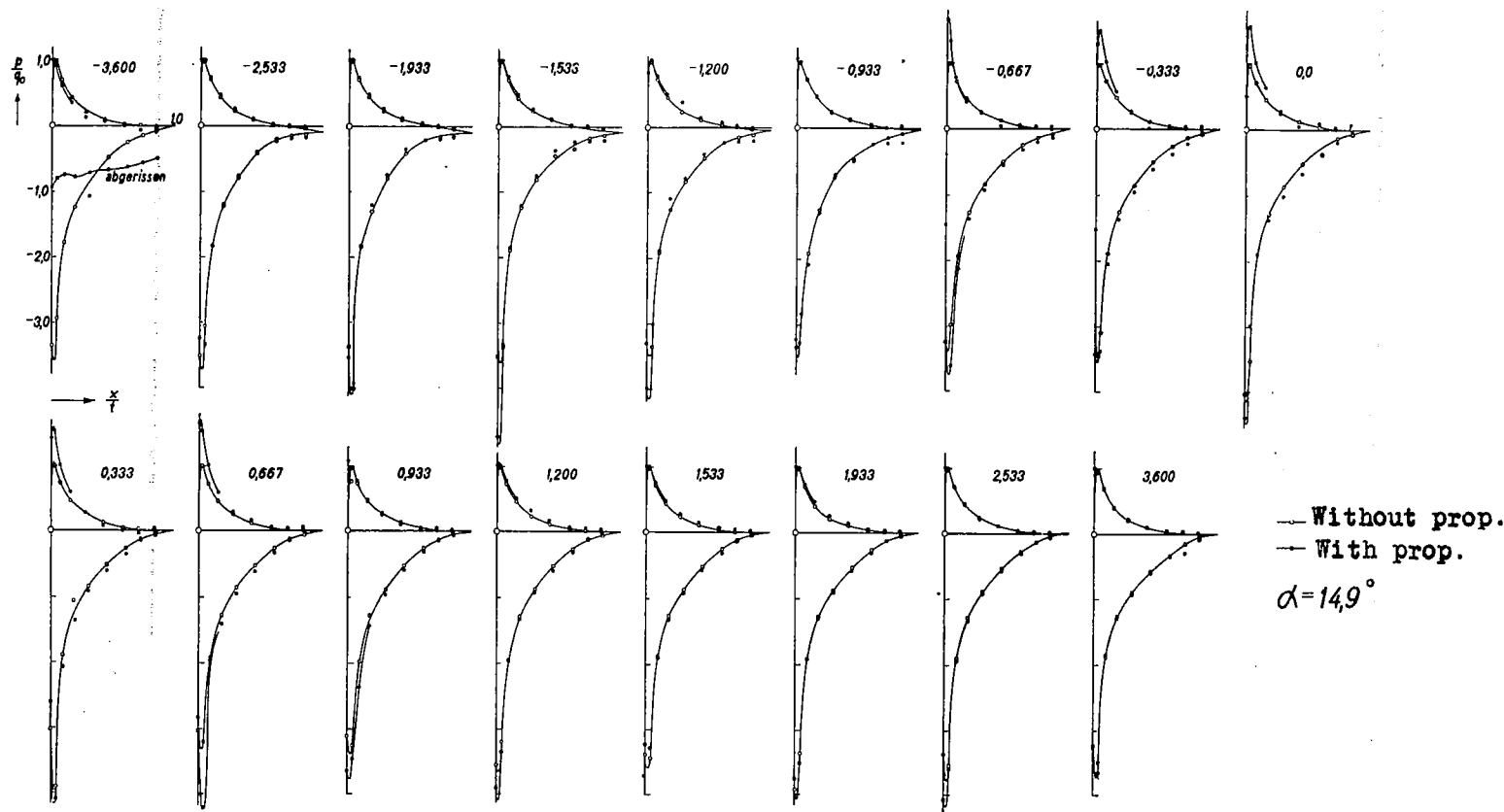
Figure 31.- Chordwise pressure distribution, α = 14.9°

Fig.31

$T_c = ?$
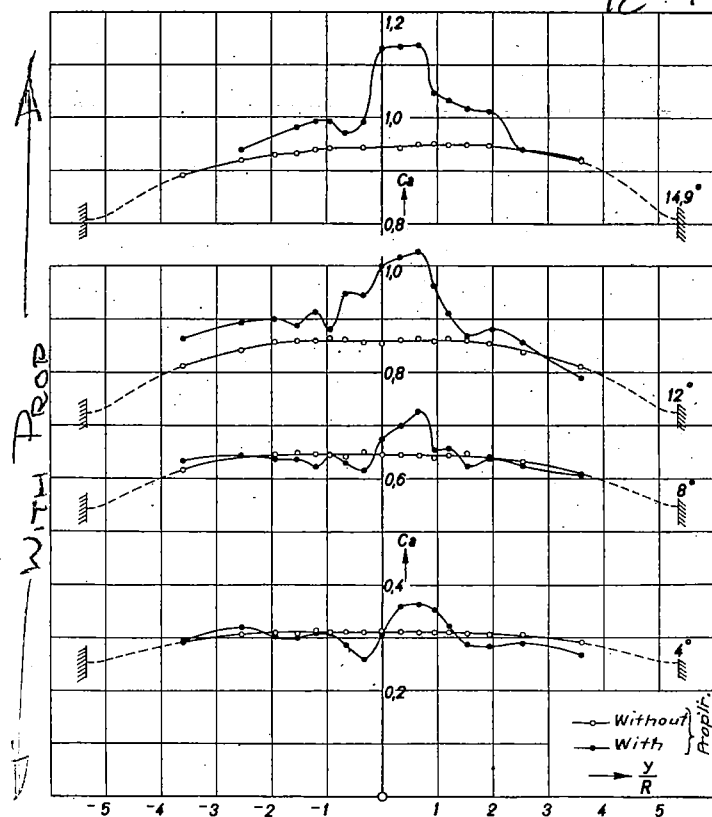
Figure 32.- Spanwise lift distribution.
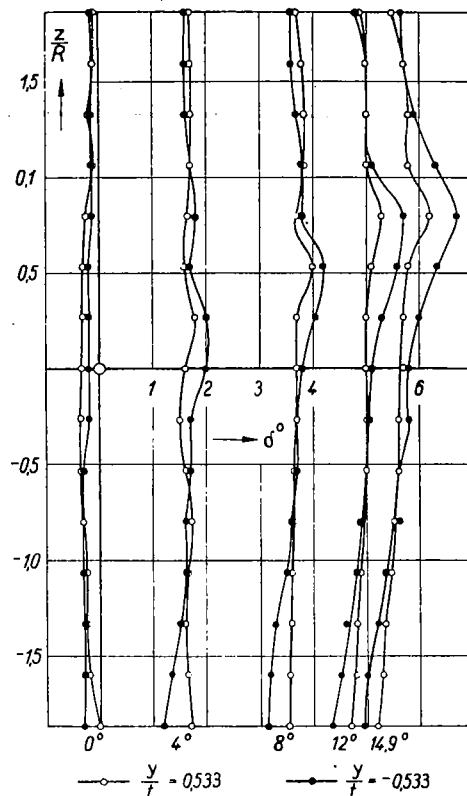
Figure 36.- Downwash behind the wing in absence of propeller slipstream.
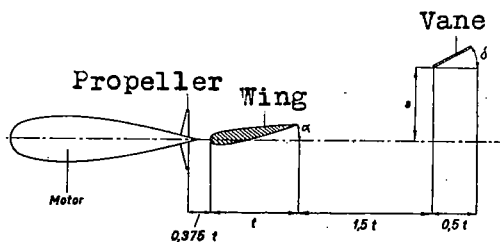
Figure 33.- Arrangement of apparatus for downwash measurements.
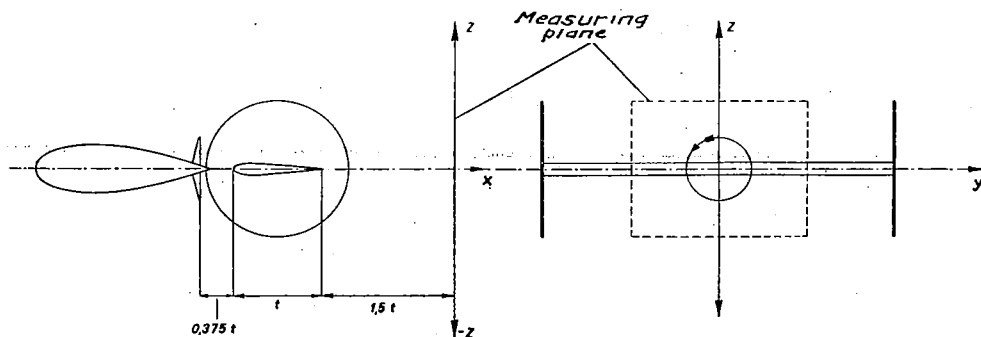
Figure 35.- Position of measuring plane.
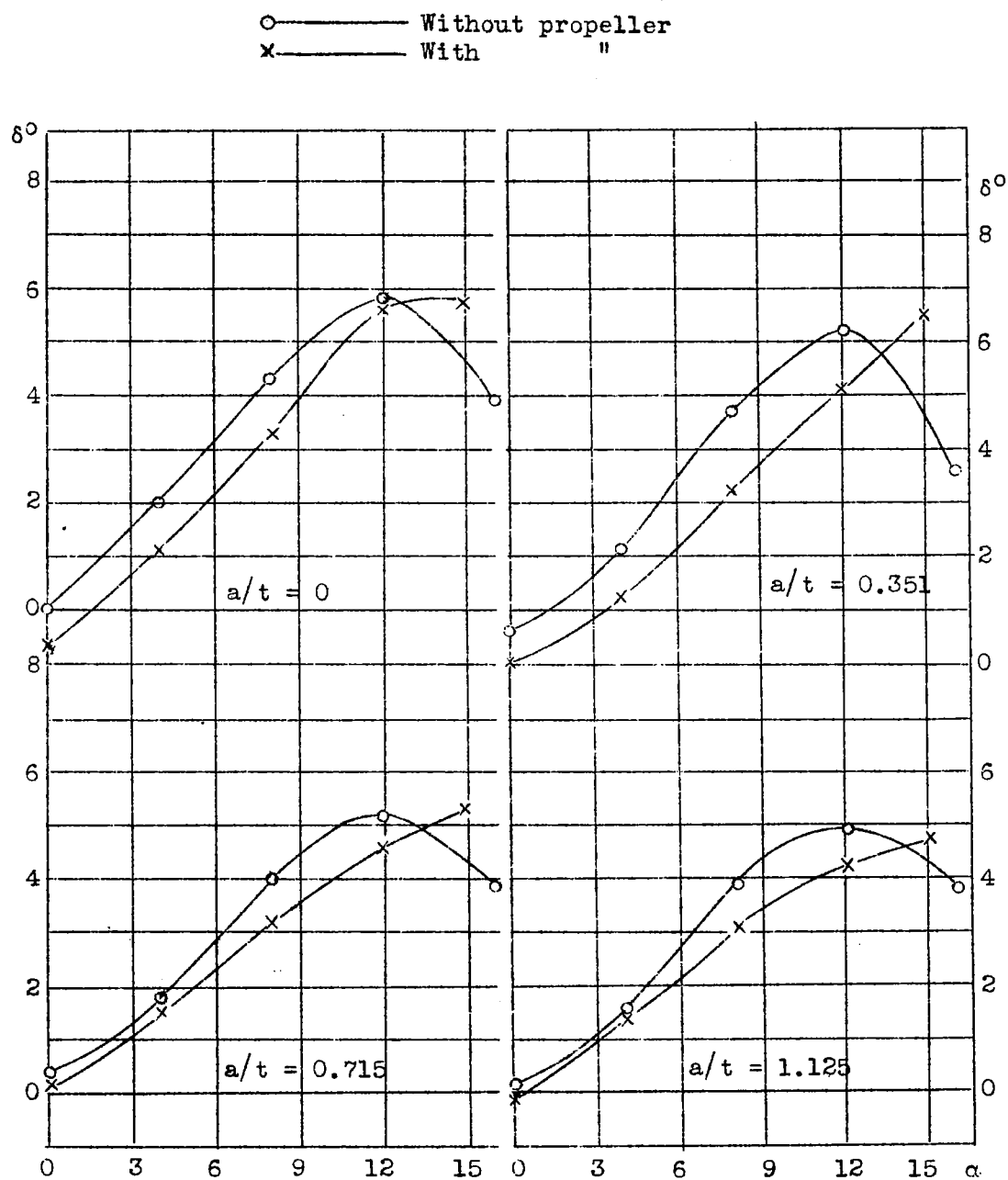
Figure 34.- Variation of downwash angle.
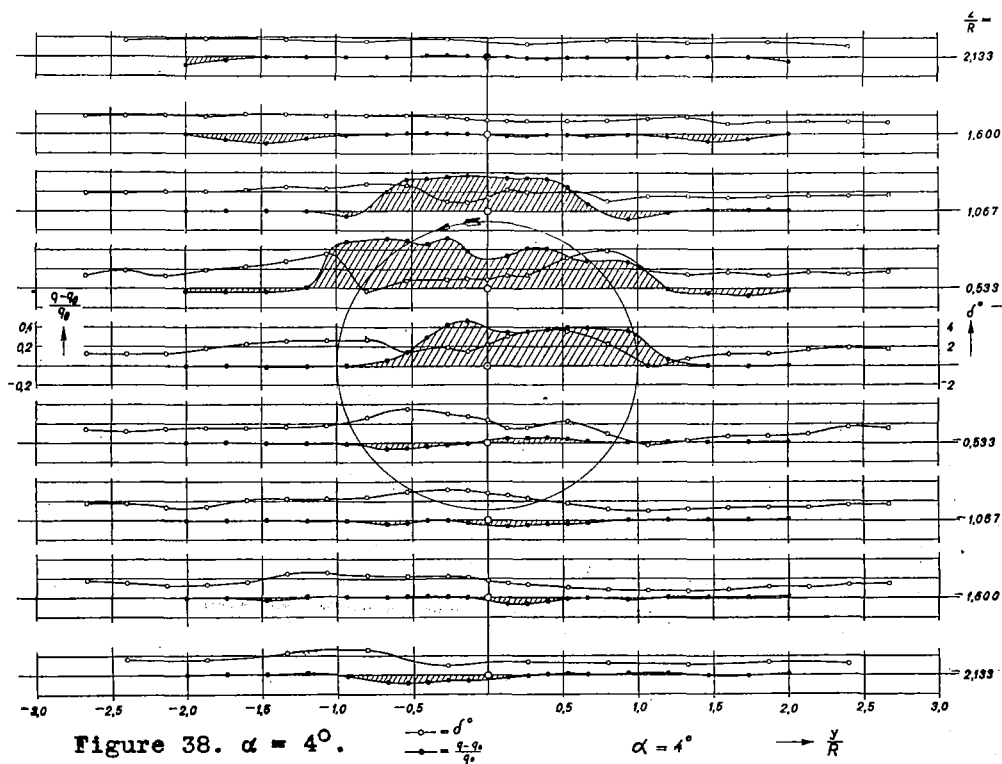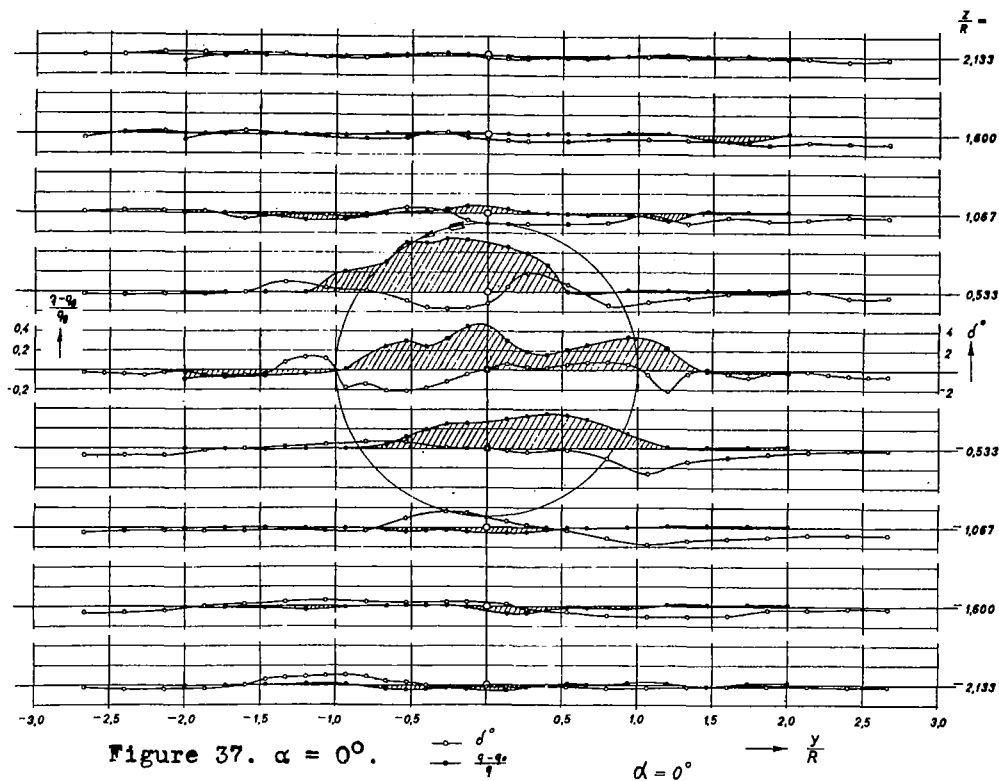
Figure 37. $\alpha = 0^\circ$.

Figure 38. $\alpha = 4^\circ$.

Downwash angle and dynamic pressure distribution.

Figure 39. α = 8°.

α = 8°

Figure 40. α = 12°.

α = 12°
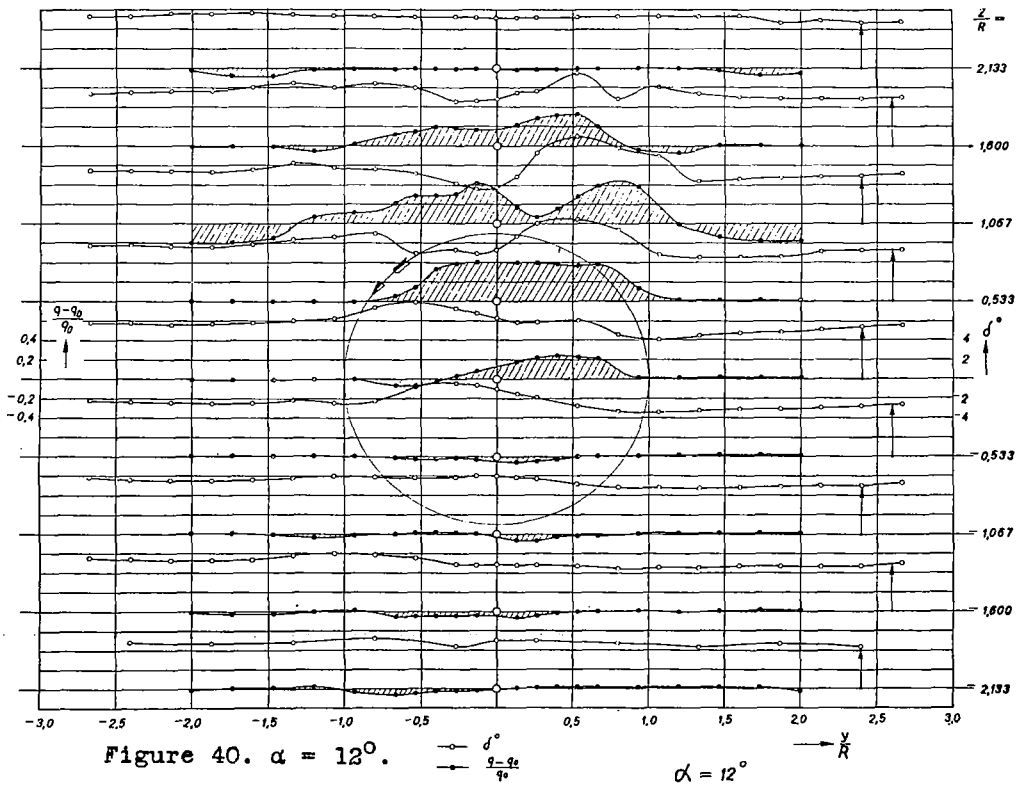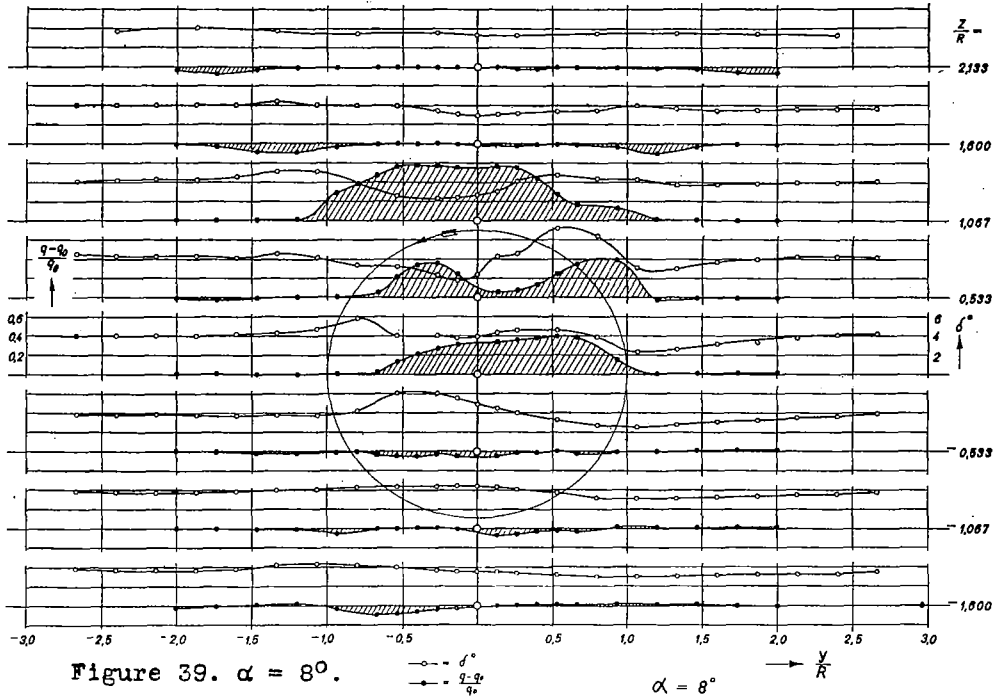
Downwash angle and dynamic pressure distribution.
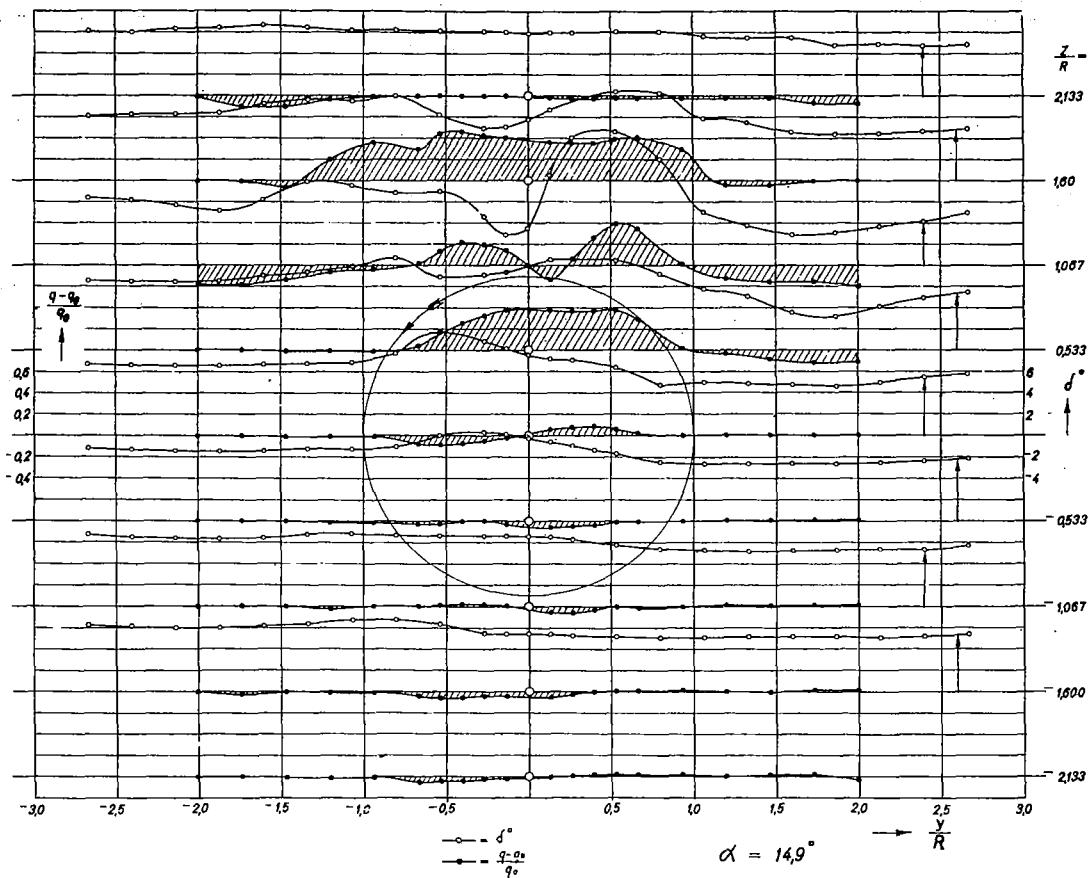
Figure 41.- Downwash angle and dynamic pressure distribution.
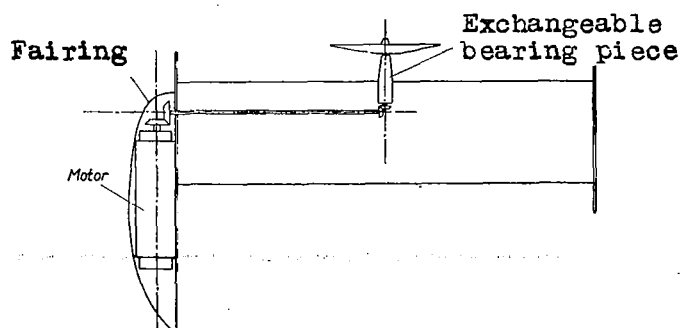
Figure 42.- Model wing with propeller.

Figure 43.- Wing with motor not   Figure 44.- Wing with motor enclosed
            enclosed in fairing.   in fairing.

Figure 77.- Test set-up for the down-
            wash measurements with
dynamic pressure sphere.
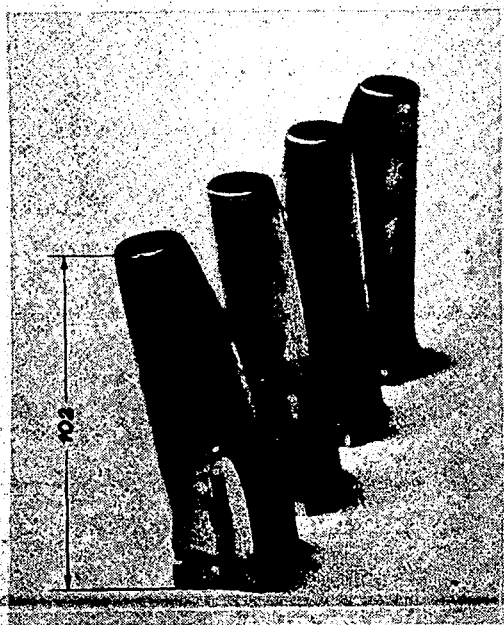
Figure 47.- Bearing pieces for
            propeller shaft.
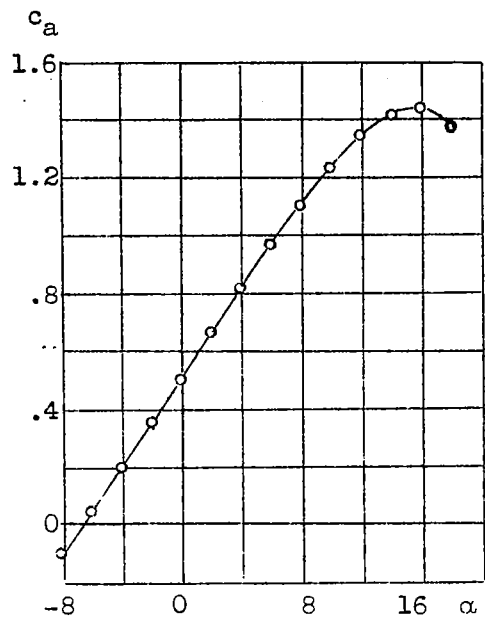
Figure 45.- Lift curve of wing alone.
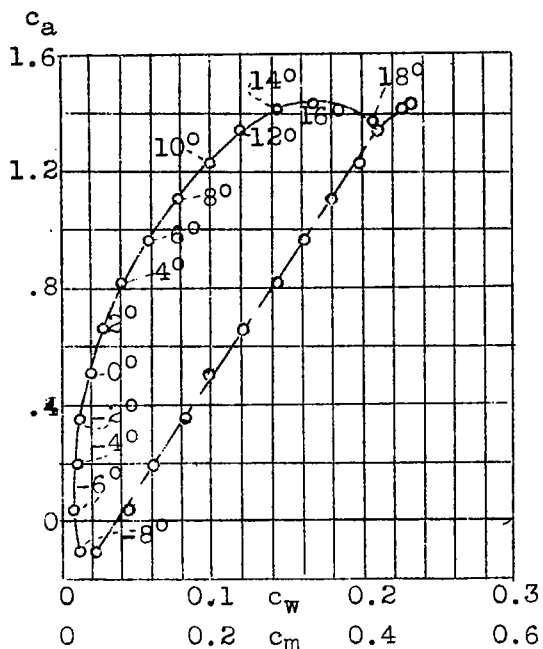
Figure 46.- Polar of wing alone.
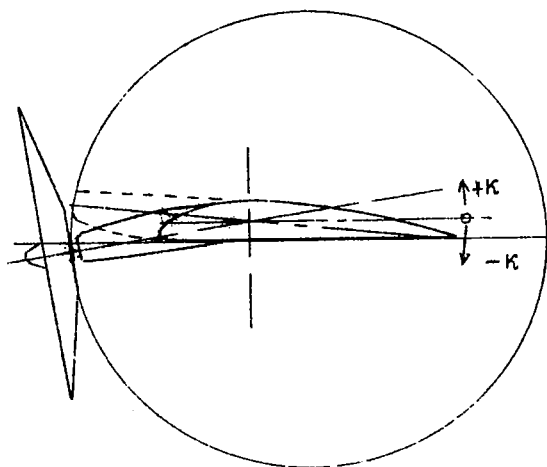
Figure 48.- Position of propeller axis $\kappa = 9^{\circ}$, dotted curve $\kappa = -6^{\circ}$.

$$k_s = \frac{thrust}{\frac{\varrho}{2}(\omega^2 R^2)(\pi R^2)} \qquad \omega = angular\ vel.$$
$$= 2\pi n$$
$$k_d = \frac{torque}{\frac{\varrho}{2}(\omega^2 R^2)(\pi R^2) R} \qquad \lambda = \frac{V}{\omega R} \cdot \frac{V}{\pi n D}$$
$$\frac{8}{\pi} T_c = c_s = \frac{k_s}{\lambda^2} \qquad \text{Figs. 49, 50, 51, 52, 53}$$

$$tan\ \beta_{0.75R} = \frac{4}{3\pi}\frac{H}{D}$$
$$= \frac{4}{3\pi} \cdot 1.0$$
$$\beta_{0.75R} = 23.0°$$

apparently
$$k_s = \frac{8}{\pi^3} C_T$$
$$k_d = \frac{8}{\pi^4} C_P$$
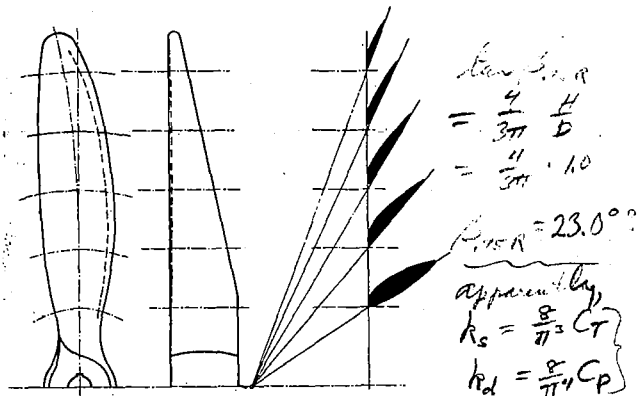
Figure 49.—Dimensioning of propeller
(American notations $S_1 F_2$
$A_2 P_1$ H/D =1.0).

$$\eta = \frac{k_s \lambda}{k_d}$$
$$\lambda = \frac{V}{\pi n D}$$
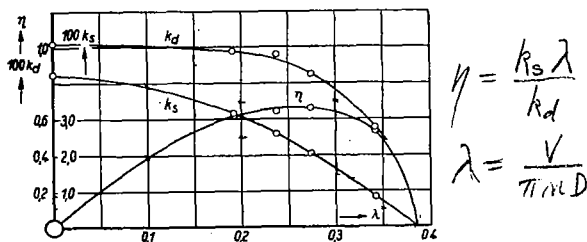
Figure 50.—Characteristics of freely
rotating propeller. $C_{y_{40}}' = .168$
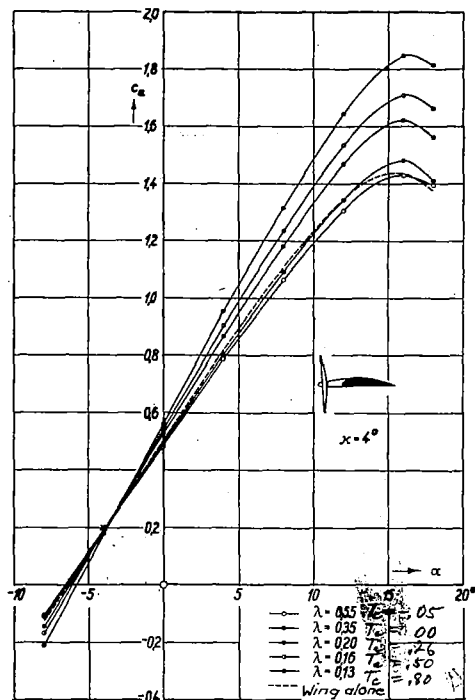
Figure 52. κ = 4°.
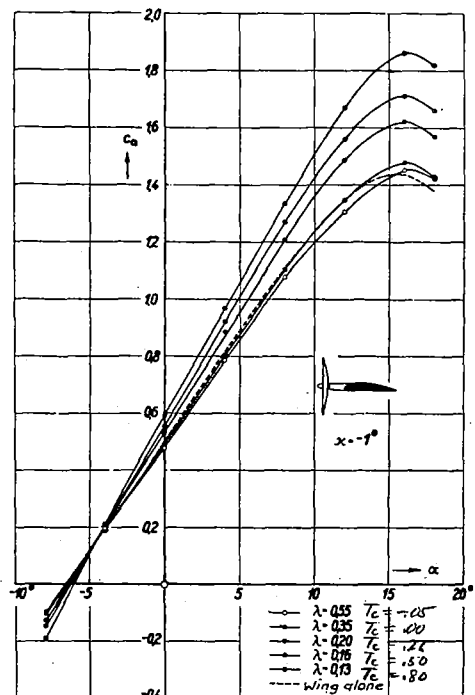
Figure 51. κ = 9°.

Figure 53. κ = —1°.

Figure 51,52,53.—Effect of propeller slipstream on lift coefficient.

Figure 54. $\kappa = -6^{\circ}$.

Figure 55. $\lambda = 0.13$.

Figures 54,55.—Effect of propeller
slipstream on lift coefficient.
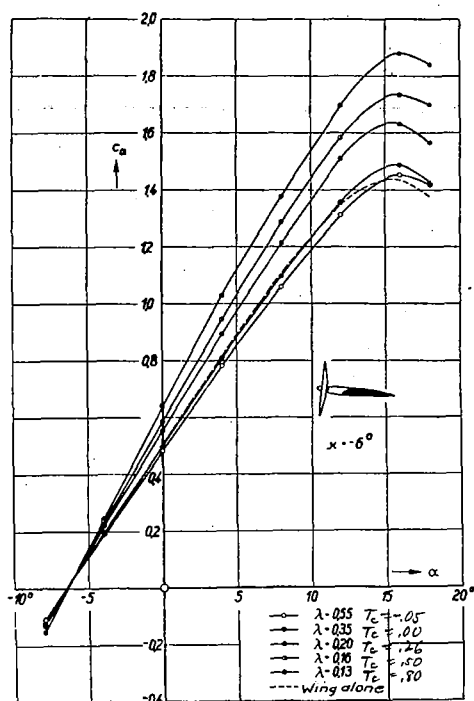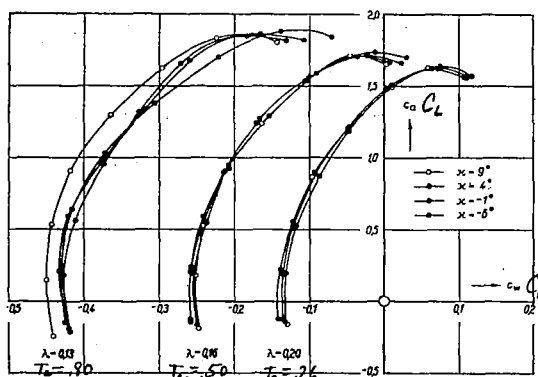
Figure 62.—Polars of wing in presence
of propeller.
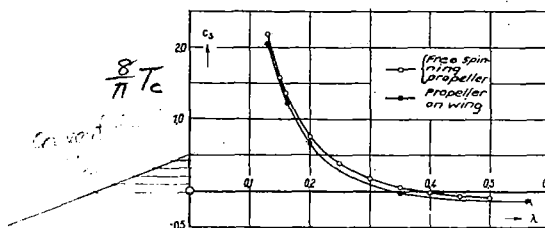
Figure 63.—Thrust coefficient as
function of λ.
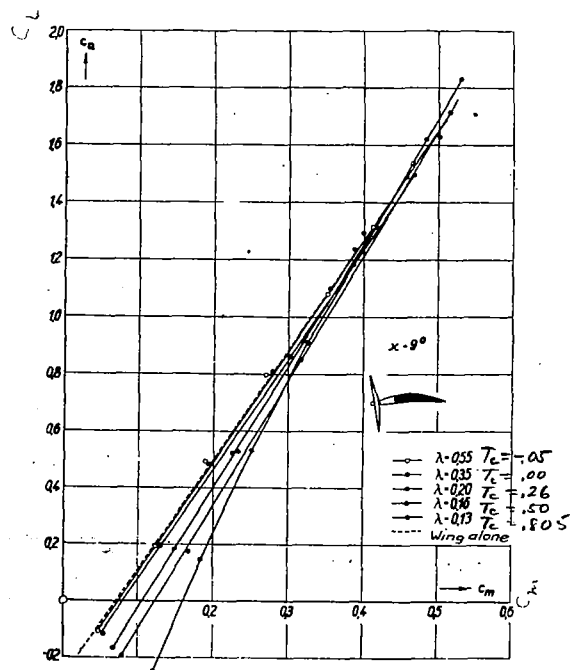
Figure 64.—Moment curves of wing in
presence of propeller.

N.A.C.A. Technical Memorandum No. 874   Figs.56,57
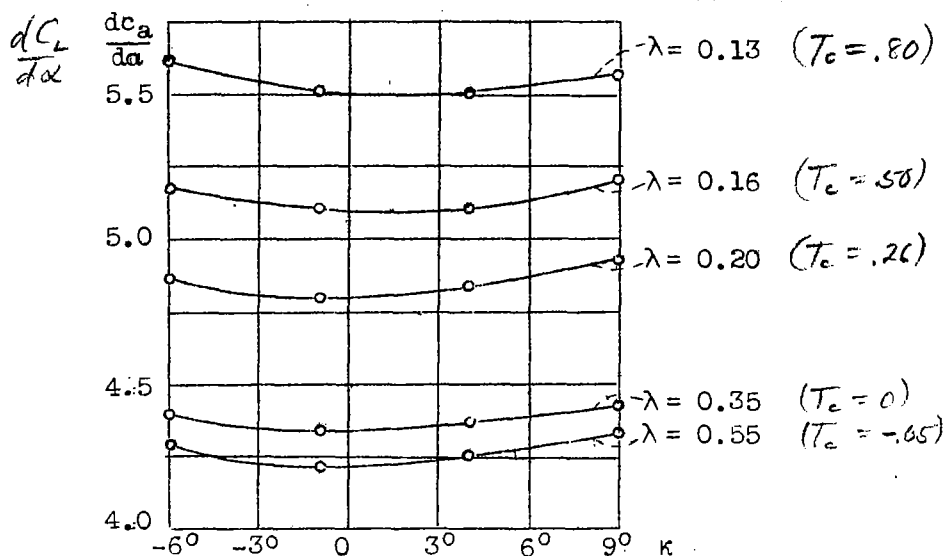
Figure 56.- Lift slope $\frac{dc_a}{d\alpha}$ as a function of κ.
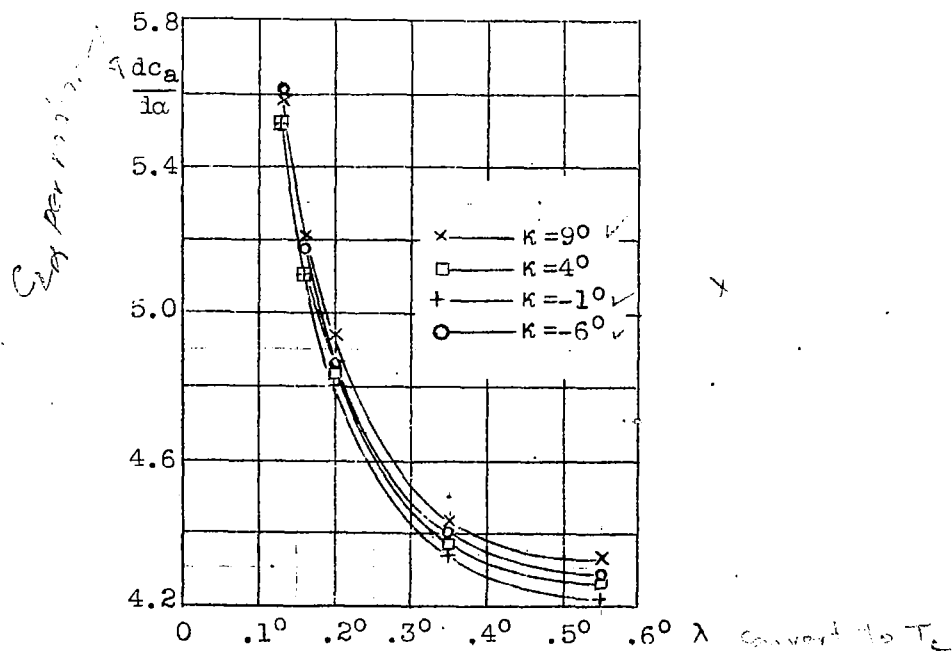
Figure 57.- Lift slope $\frac{dc_a}{d\alpha}$ as a function of λ.
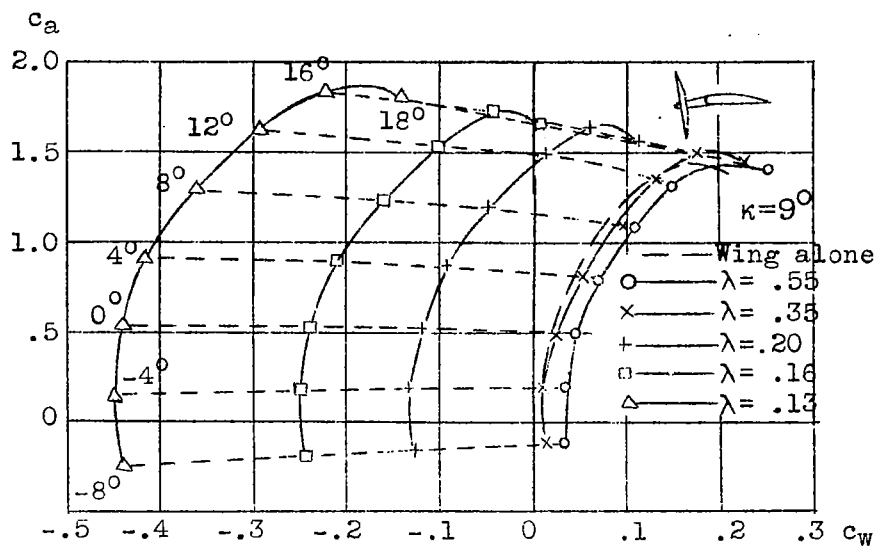
Figure 58.- Polars of wing in presence of propeller, $\kappa = 9^o$.
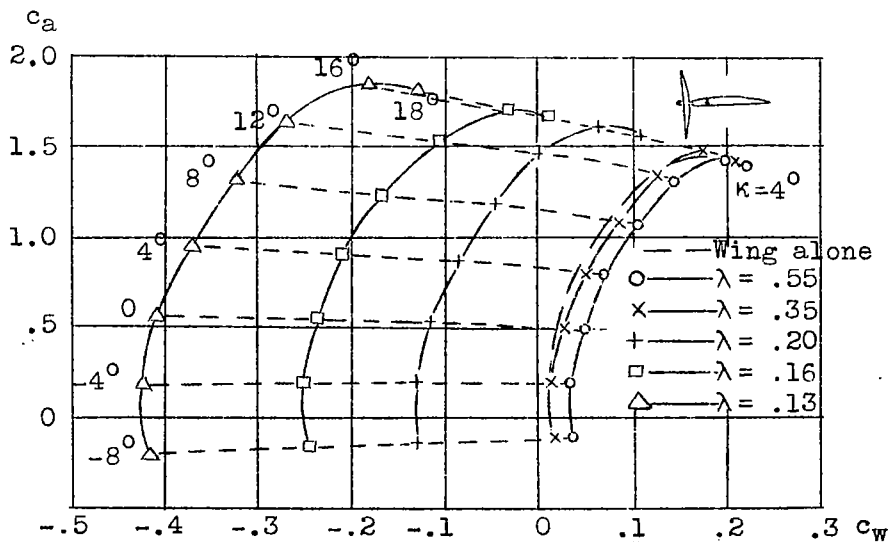
Figure 59.- Polars of wing in presence of propeller. $\kappa = 4^o$.
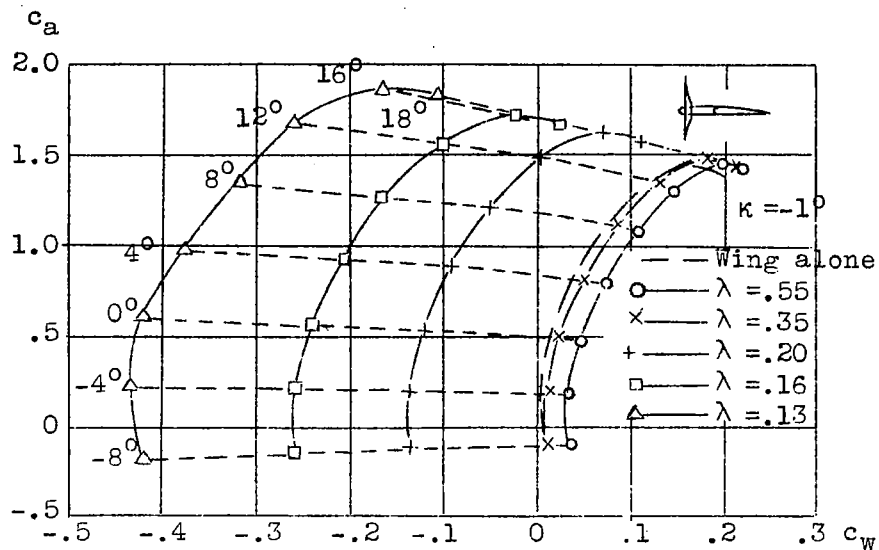
Figure 60.- Polars of wing in presence of propeller, $\kappa = -1°$.
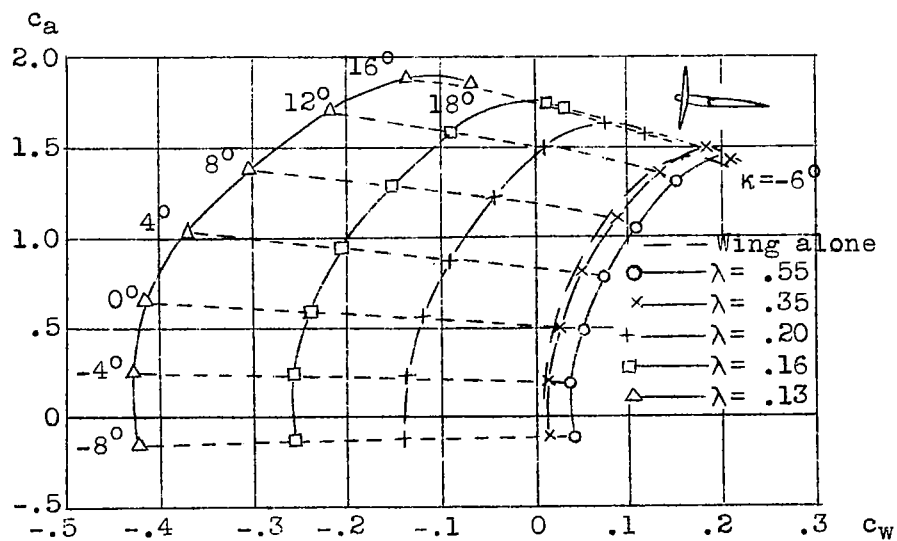
Figure 61.- Polars of wing in presence of propeller, $\kappa = -6°$.
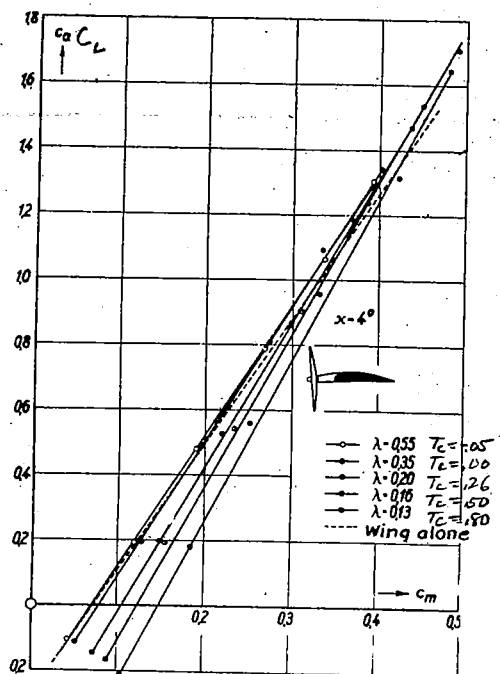
Figure 65. κ=4°
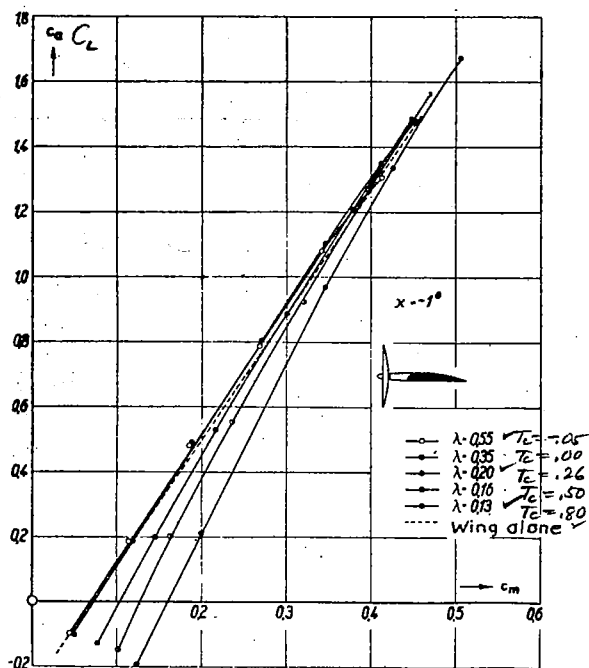
Figure 66. κ=-1°
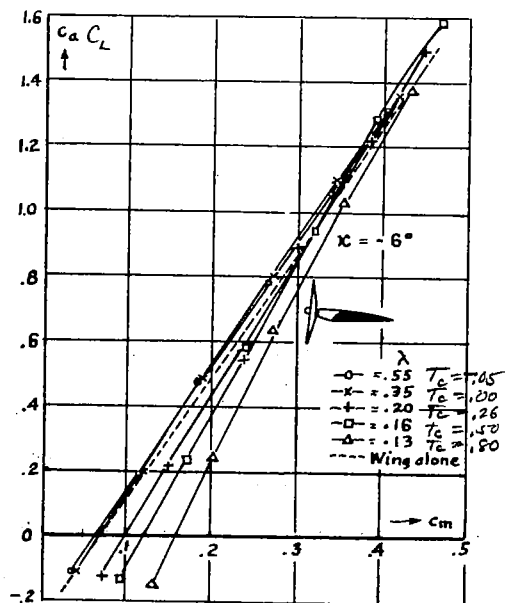
Figure 67. κ=-6°
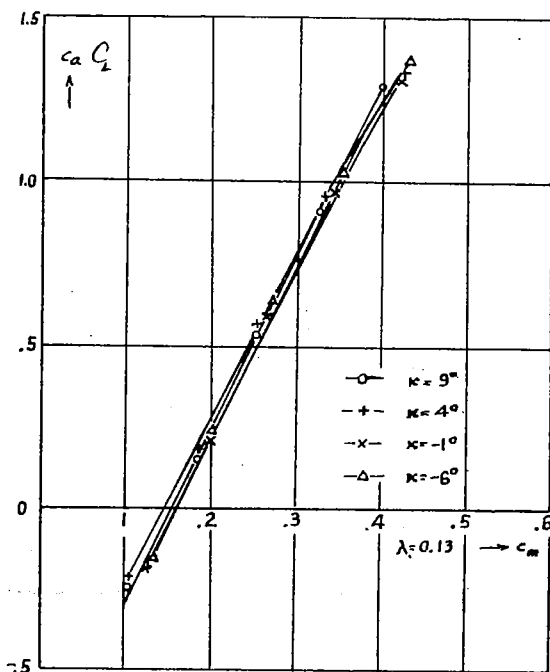
Figure 68. λ=0.13 $(T_c = ,80)$

Moment curves of wing in presence of propeller.

$$\frac{dc_m}{dc_a}$$

$$-\frac{dC_m}{dC_L}$$

Wing alone $(\lambda = \infty)$

$$\lambda = \frac{V}{\pi n D}$$
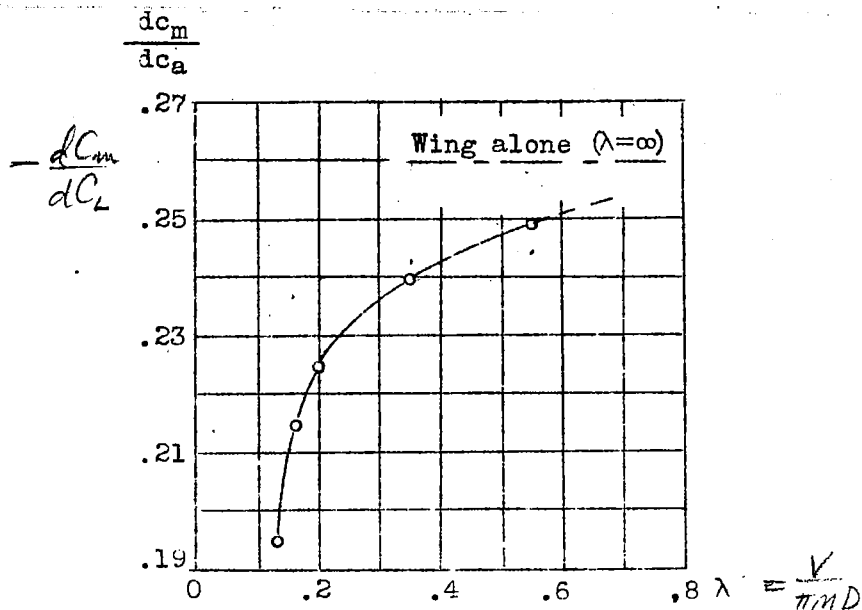
Figure 69.- Stability coefficient $\dfrac{dc_m}{dc_a}$ of wing in presence of propeller.

$$\frac{dc_m}{d\lambda}$$

○———— $\kappa = 9°$
✕———— $\kappa = 4°$
+———— $\kappa = -1°$
△———— $\kappa = -6°$
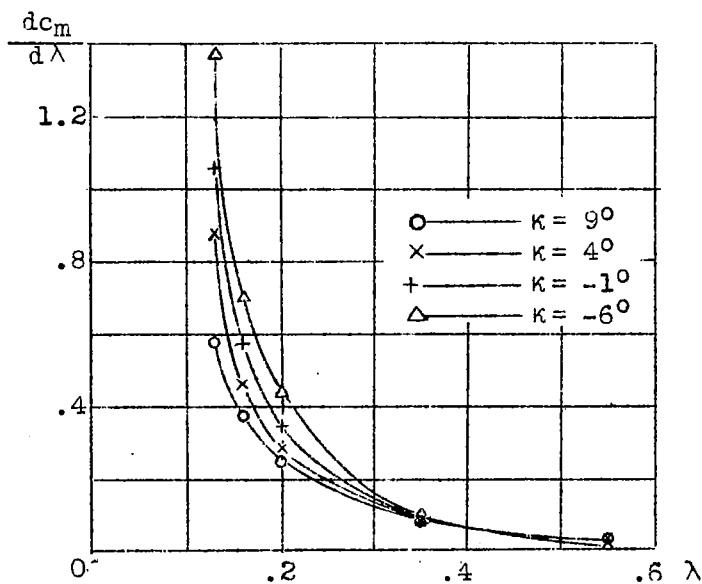
Figure 70.- Variation of $\dfrac{dc_m}{d\lambda}$ with λ and κ.
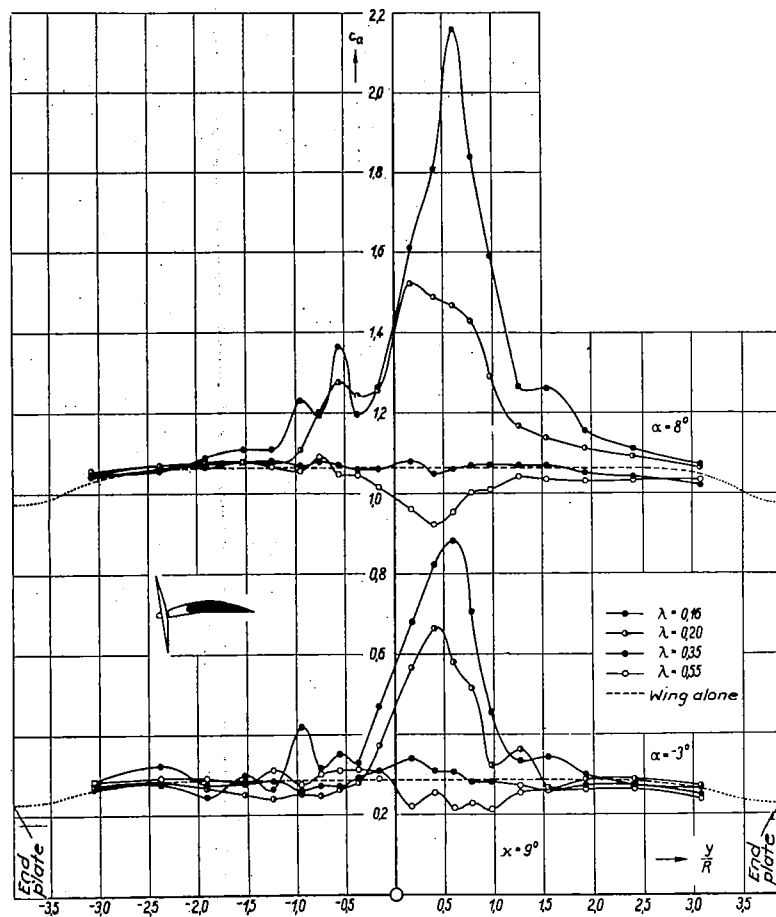
Figure 71. κ = 9°.
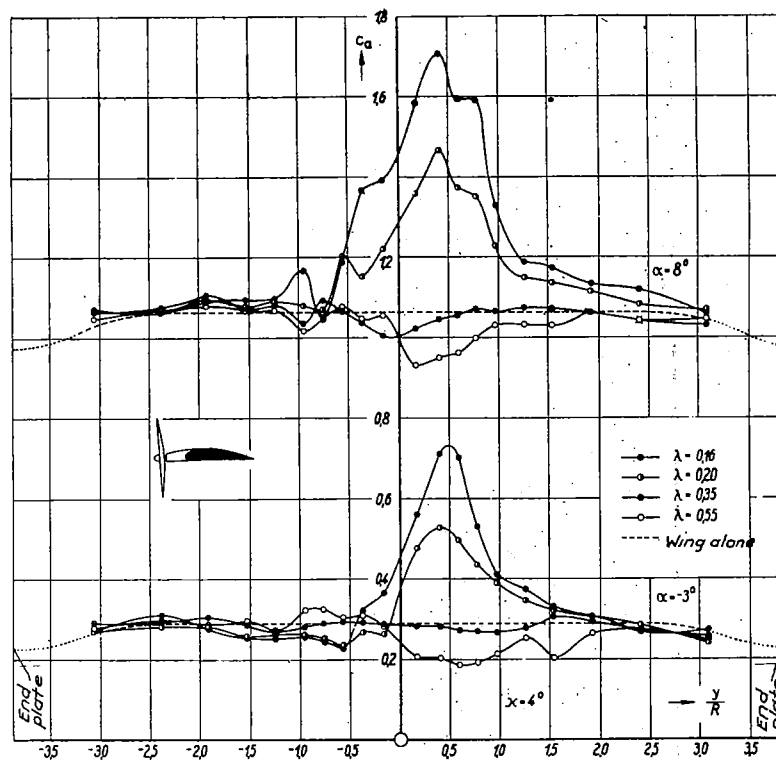
Figure 72. κ = 4°.

Spanwise lift distribution.
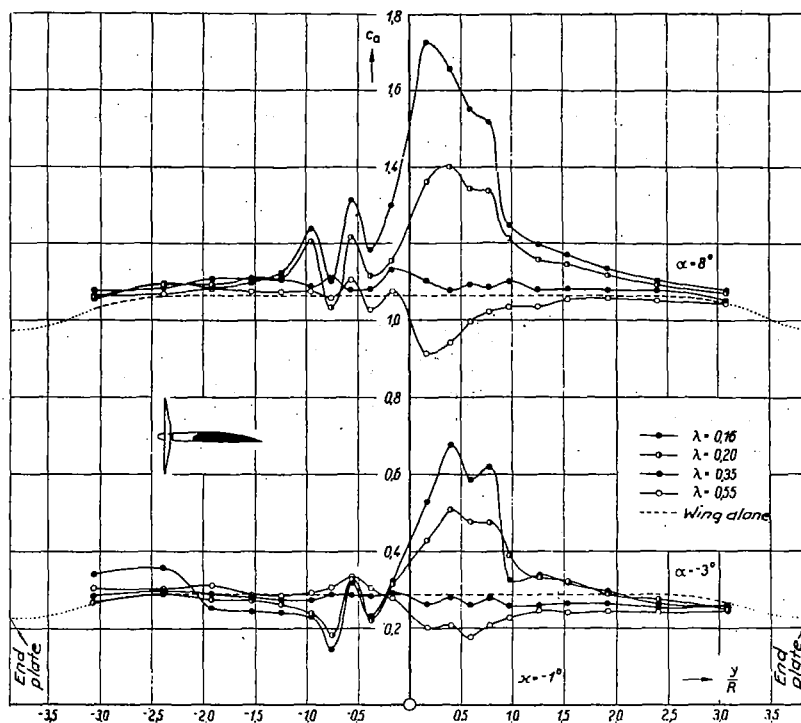
Figure 73. $\kappa = -1^{\circ}$.
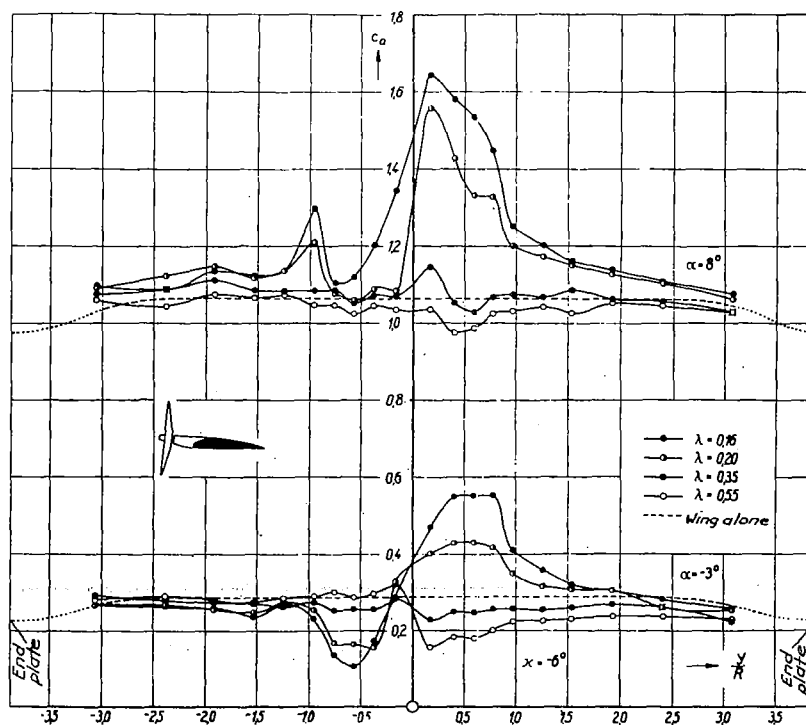
Figure 74. $\kappa = -6^{\circ}$.

Spanwise lift distribution.
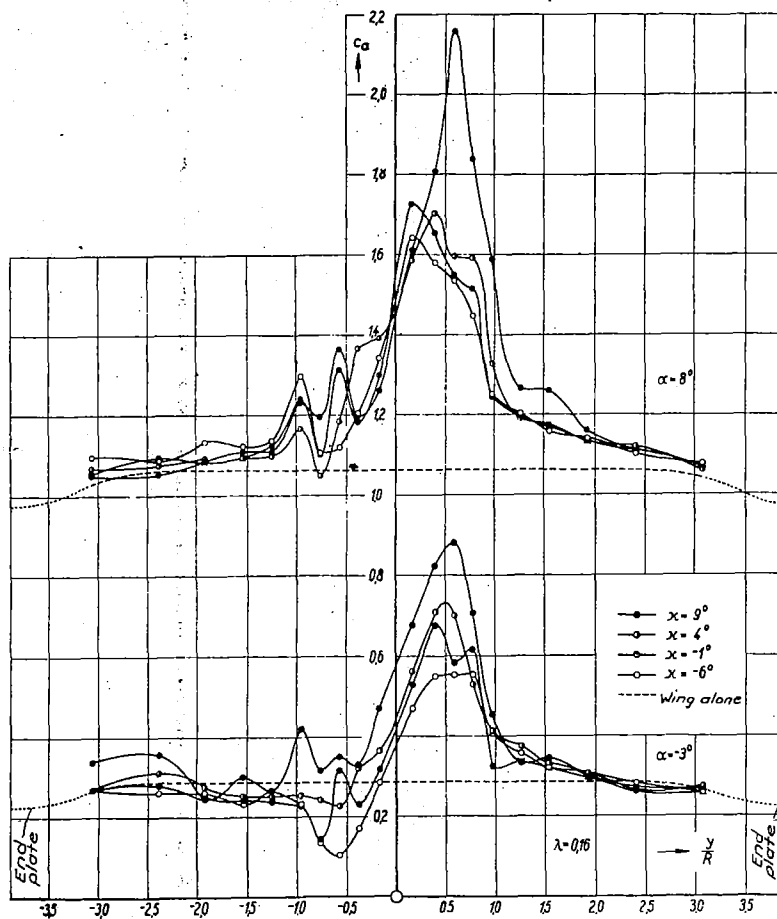
Figure 75.-Spanwise lift distribution. $\lambda = 0.16$
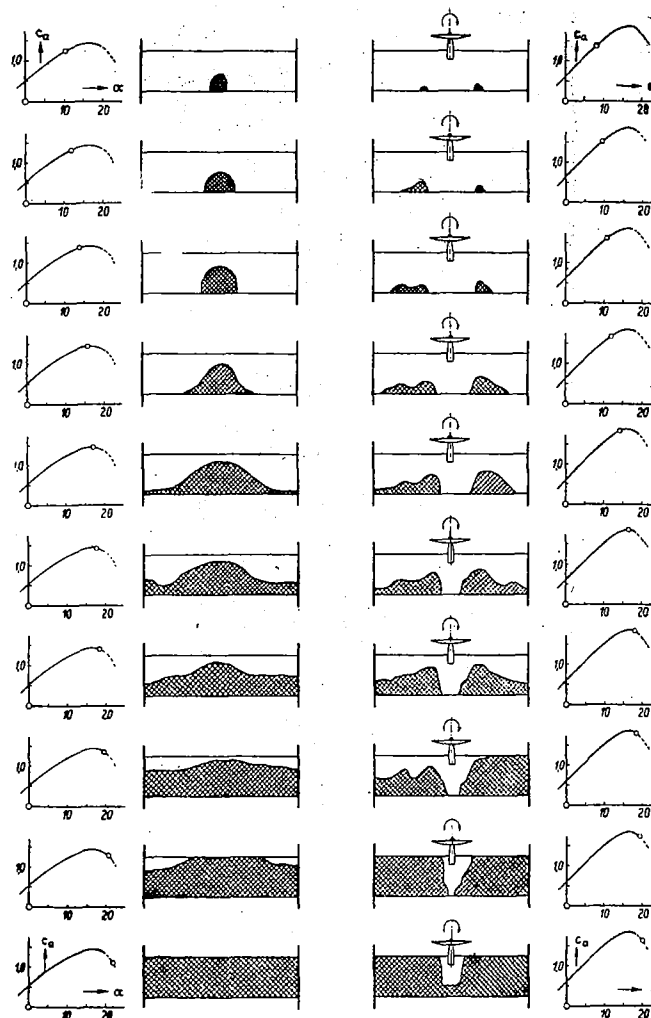
Figure 76.-Spread of flow separation over the wing.
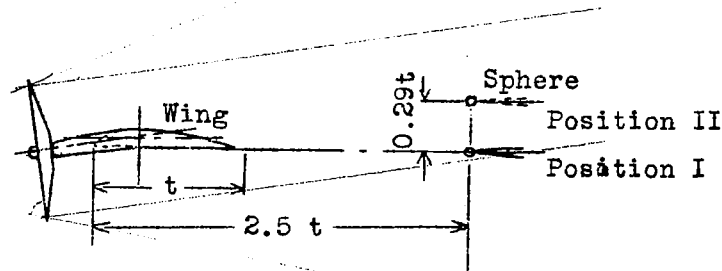
Figure 78.- Arrangement for downwash measurements.
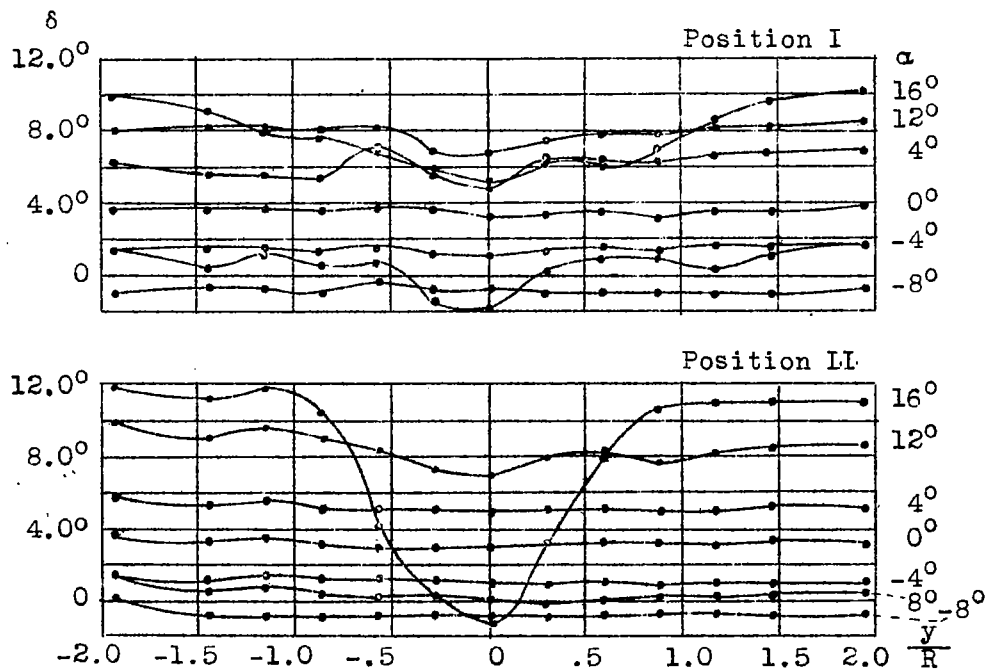
Figure 79.- Downwash behind wing without propeller.
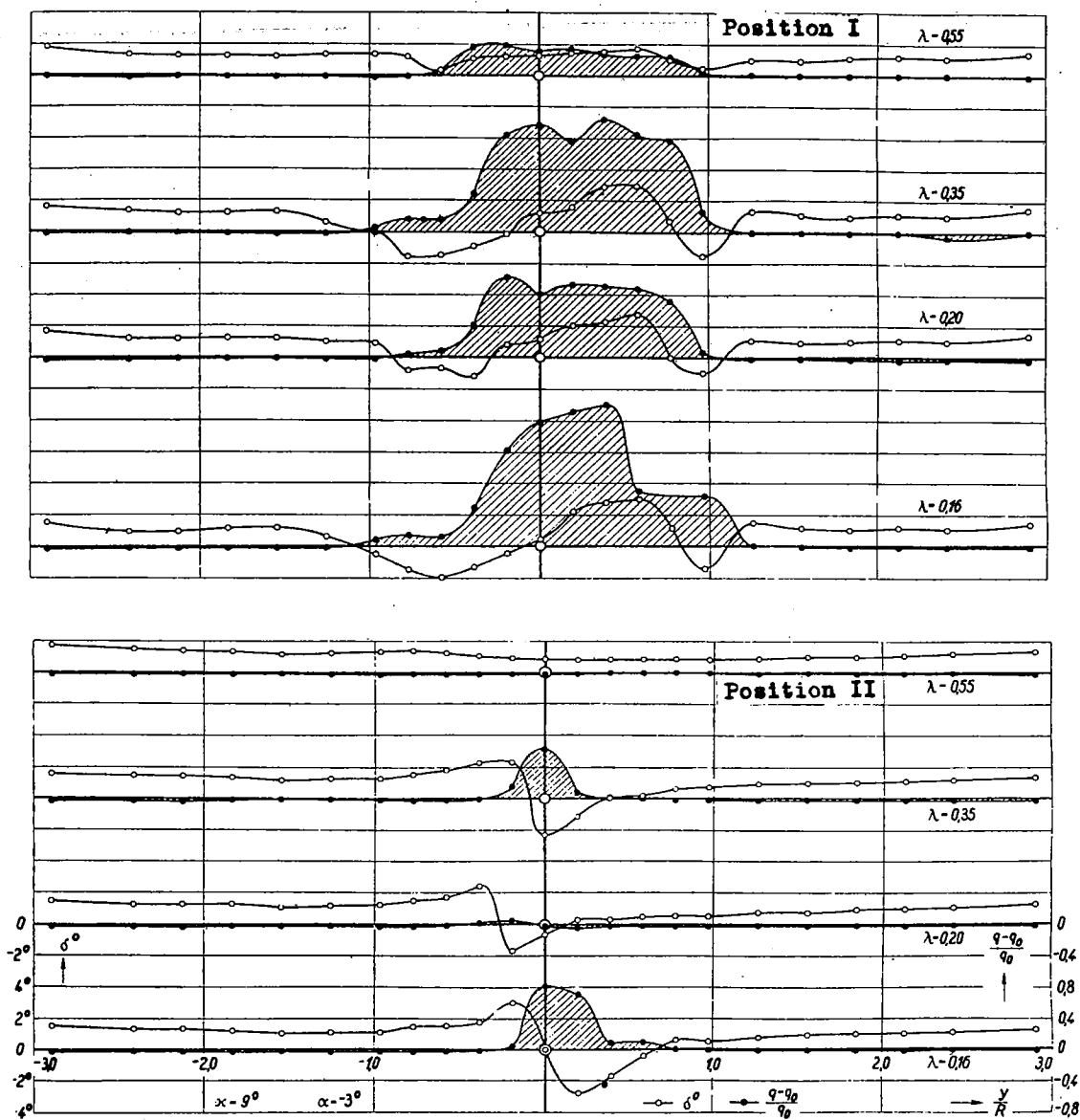
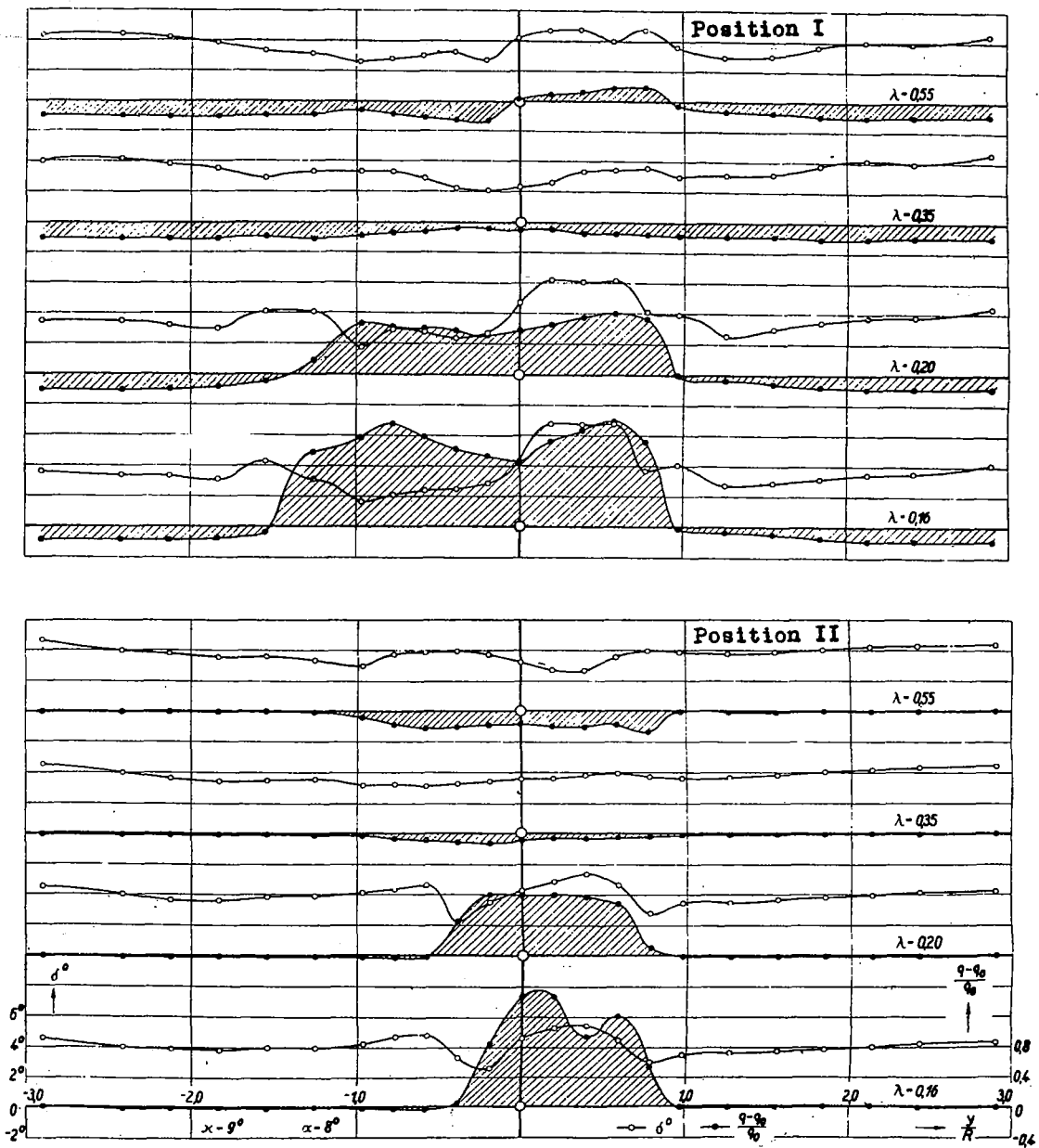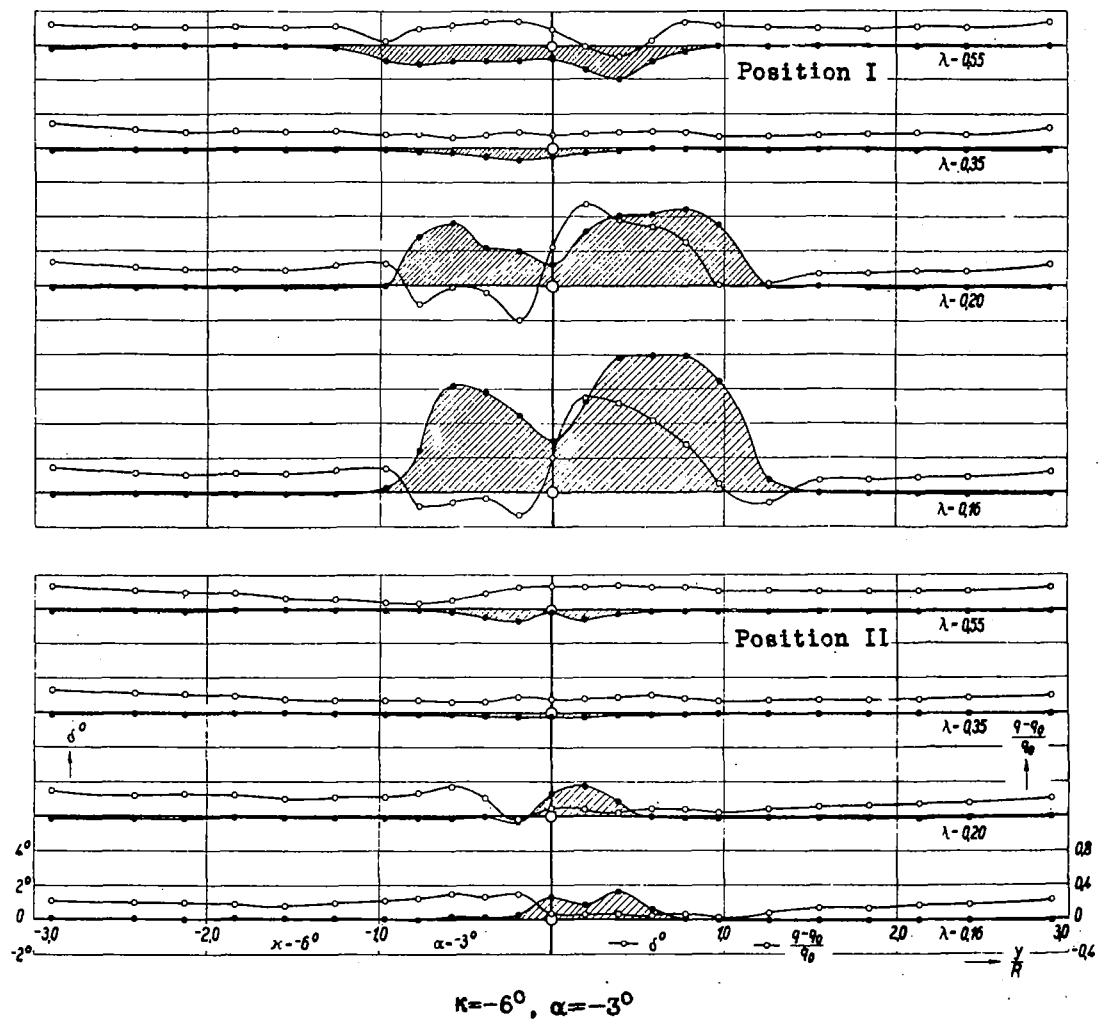Figure 80.- Downwash distribution with propeller. $\kappa = 9°$, $\alpha = -3°$

Figure 81.- Downwash distribution with propeller. κ=9°, α=8°
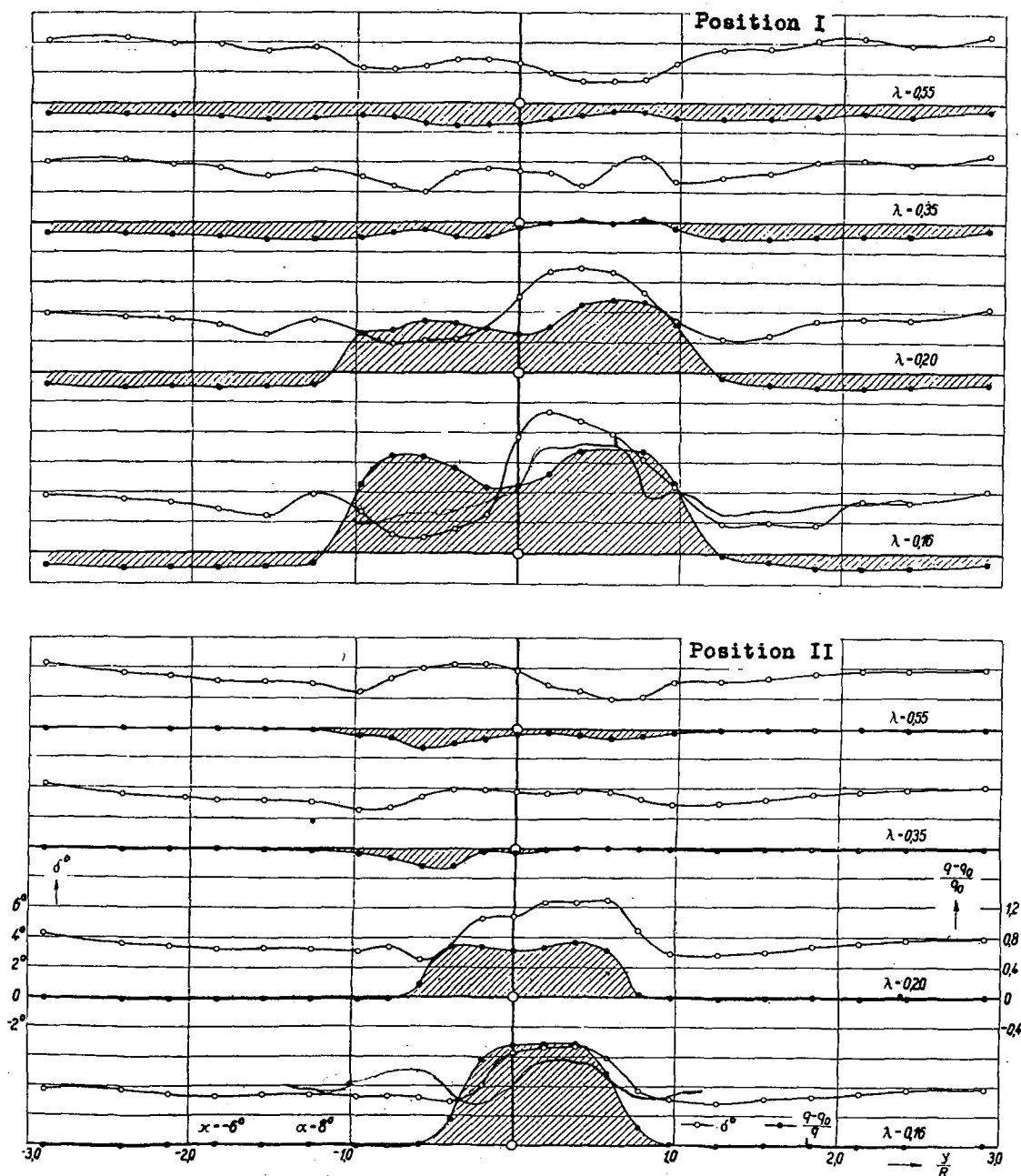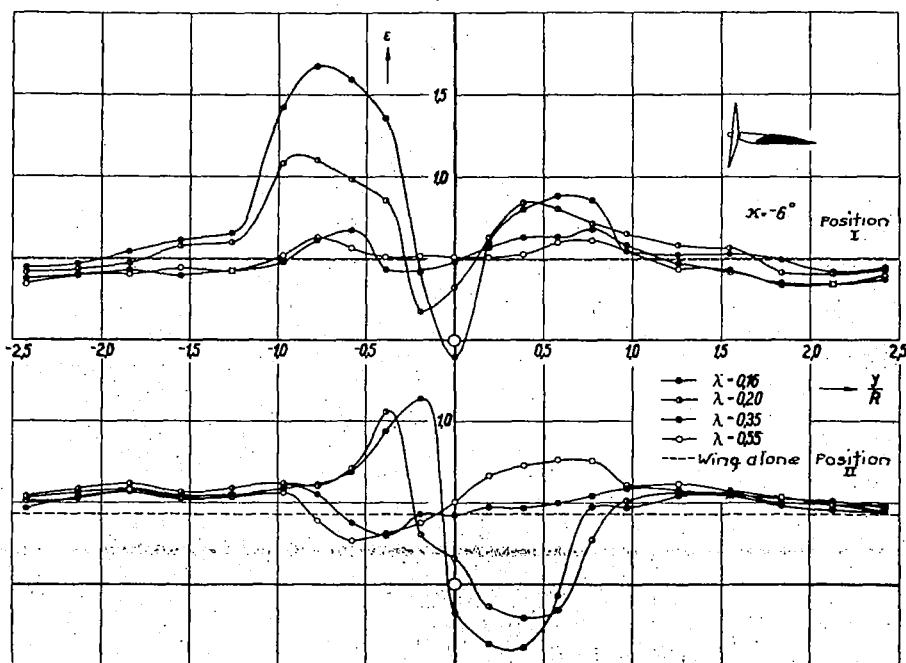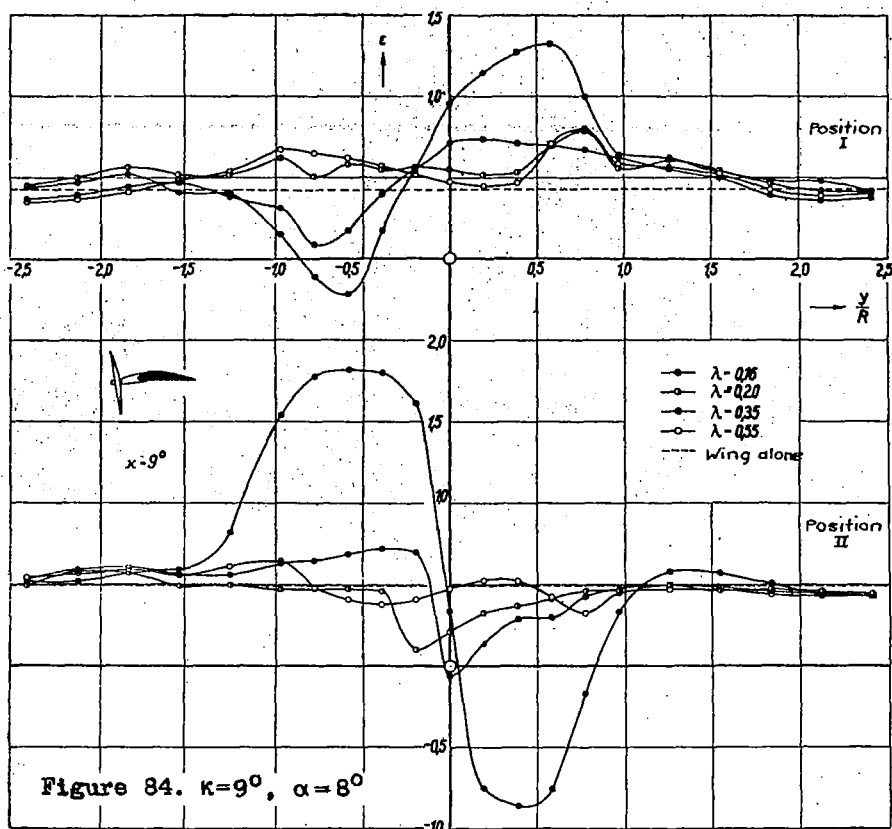
Fig. 82

$\kappa = -6^{\circ}, \ \alpha = -3^{\circ}$

Figure 82.- Downwash distribution with propeller.

Figure 83.- Downwash distribution with propeller. $\kappa = -6°$, $\alpha = 8°$

Figure 84.　κ=9°,　α=8°

Figure 85.　κ=-6°,　α=8°

Spanwise variation of ∈, the "tail flow efficiency".